



# MASTERARBEIT / MASTER'S THESIS

Titel der Masterarbeit / Title of the Master's Thesis

“Degradation of Polymers used  
as Drag Reducing Agents”

verfasst von / submitted by

Lukas Brandfellner, BSc

angestrebter akademischer Grad / in partial fulfilment of the requirements for the degree of  
Master of Science (MSc)

Wien, 2020 / Vienna 2020

Studienkennzahl lt. Studienblatt /  
degree programme code as it appears on  
the student record sheet:

A 066 862

Studienrichtung lt. Studienblatt /  
degree programme as it appears on  
the student record sheet:

Masterstudium Chemie

Betreut von / Supervisor:

Univ.-Prof. Dr. Alexander Bismarck

Mitbetreut von / Co-Supervisor:

Dipl.-Phys. Dr. Hans Werner Müller



## Acknowledgements

I would like to thank my supervisors Alexander Bismarck and Hans Werner Müller. Thank you for the opportunity to perform this work in your group and thank you for all the discussions, support and corrections.

I want to thank all members of the PaCE-group. I am glad to be part of this group and can count on the input and the help of all of you.

At last I also want to thank my family. Without you I would have not been able to do this.



## Contents

1. Introduction.....	6
1.1 Application and limitations of polymeric drag reducing agents .....	6
1.2 Project aim: Long term characterisation of DRAs in pipe-flow .....	7
1.3 Theoretical background.....	8
1.3.1 Fluids in pipes .....	8
1.3.2 Drag reduction in turbulent pipe flow.....	10
1.3.3 Degradation of polymeric drag reducing agents.....	10
1.3.4 Behaviour of fluids in Couette-Taylor-flow .....	11
1.3.5 Characteristics of the molecular weight distribution of polymers.....	12
1.3.6 Gel Permeation Chromatography .....	13
1.4 Properties of polyethylene oxide .....	14
2. Experimental Methods .....	15
2.1 Materials.....	15
2.2 Drag reduction measurements in a pipe flow facility .....	15
2.3 Measurements of apparent viscosity in a rheometer .....	18
2.4 Execution of molecular weight measurements using GPC.....	19
2.5 Experiments performed .....	20
2.5.1 Reference measurements .....	20
2.5.2 Solutions of polyethylene oxide .....	21
3. Results and Discussion .....	23
3.1 Flow characterisation in ViEDRA .....	23
3.2 Drag reduction in long term experiments.....	24
3.3 Flow characterisation in the Rheometer.....	27
3.4 Molecular weight of sheared polyethylene oxide solutions .....	28
3.5 Untangling ageing and degradation .....	33
3.6 Comparison of PEO with different molecular weight .....	36
3.7 Comparison of the measured polymer degradation with Brostow's model.....	38
4. Summary and Outlook.....	40
Bibliography.....	41
Appendix A: GPC calibration.....	44
Appendix B: Detailed results in Couette-Taylor flow .....	45
Appendix C: Age mapping .....	47
English Abstract.....	51
Deutsche Zusammenfassung.....	52

## Abbreviations

DHR	Discovery Hybrid Rheometer
DI water	Deionized water
DPT	Differential Pressure Transducer
FSD	Flow Straightening Device
GPC	Gel Permeation Chromatography
HPLC	High Pressure Liquid Chromatography
LALS	Low Angle Light Scattering detector
PEG	Polyethylene Glycol
PEO	Polyethylene Oxide
RALS	Right Angle Light Scattering detector
RI	Refractive Index detector
ViEDRA	Vienna Experiment for Drag Reducing Agents
VIS	Viscosity detector
wppm	weight parts per million

## Symbols

$\alpha$	Mark-Houwink parameter
$\dot{\gamma}$	shear rate
$c$	concentration
$d$	pipe diameter
$\Delta p$	pressure drop

$\Delta p_s$	pressure drop of the pure solvent
$\mathcal{D}_M$	molecular weight dispersity
DR	drag reduction
$f$	Fanning friction factor
$f_s$	Fanning friction factor of the pure solvent
$\eta$	dynamic viscosity
$\dot{\eta}$	apparent viscosity
$h_0$	rate constant in Brostow's model
$m$	mass
$M_\eta$	viscosity average molecular weight
$M_n$	number average molecular weight
$M_p$	molecular weight at the peak of the GPC chromatogram
$M_w$	weight average molecular weight
$\rho$	density
$\tau$	shear stress
$\ell$	age of the polymer solution
$t$	time
$U$	flow velocity
$V$	volume
$V_R$	retention volume
$W$	number of weak points in the polymer chain

## 1. Introduction

### 1.1 Application and limitations of polymeric drag reducing agents

In the flow of fluids at high Reynolds-numbers, turbulence causes a dissipation of energy via the formation of vortices, resulting in a force counteracting the flow. With increasing flow velocity, the drag increases much stronger than in laminar flow of the same velocity. This is relevant in systems, where large amounts of fluid are pumped (e.g. an oil pipeline) or for an object that is moving through a fluid at high velocity (e.g. a ship moving through the ocean). In order to maintain the desired velocity, a constant energy input is required. The drag caused by turbulence is directly responsible for a major part of the energy consumption in these applications.

Polymeric drag reducing agents (DRAs) are soluble, high molecular weight molecules that can reduce this drag. When small amounts (in the range of 100 wppm) of a polymer with long, flexible chains are dissolved in a liquid, the pressure drop encountered at high Reynolds numbers is significantly smaller for the polymer solution than for the pure solvent. This effect was first described in 1948 by Toms<sup>[1]</sup> and has triggered extensive theoretical and practical research. Drag reduction up to 80% has been reported in the literature<sup>[2]</sup> and numerous applications have been developed. Polymeric drag reducing agents save energy and enable high flow rates in oil pipelines,<sup>[3]</sup> airplane tanks,<sup>[4]</sup> irrigation systems,<sup>[5]</sup> sewers,<sup>[6]</sup> firefighting,<sup>[7]</sup> and in hydraulic fracturing.<sup>[8]</sup> In all these applications the benefits outweigh the costs of the additives.

Numerous studies have been performed in order to investigate the behaviour of polymeric drag reducing agents and explain the drag reduction mechanism. Most experiments were conducted either in circular systems like external flow in rotating disk apparatuses<sup>[9]</sup> and Taylor flow between rotating concentric cylinders<sup>[10, 11]</sup> or in pipe and channel flow in specifically constructed facilities<sup>[12, 13, 14]</sup>. While the circular systems are easier to handle, only experiments with pipe-flow facilities correctly resemble the flow encountered in most applications.<sup>[14]</sup> The nature of turbulent flow strongly depends on the geometry of the system; the turbulence structure depends on the boundary conditions. Even in pipe-flow facilities the behaviour of drag reducing agents depends on the geometry of the pipe,<sup>[15]</sup> sharp edges in the flow-path,<sup>[16]</sup> the method of introducing the polymer into the liquid<sup>[17]</sup> and the inclusion of pumps.<sup>[18]</sup>

In recent years, numerical simulations improved the understanding of the mechanisms which cause drag reduction.<sup>[19, 20]</sup> Model systems are able to explain phenomena, encountered in the interaction of polymeric drag reducing agents with turbulent flow, based on theoretical assumptions. However, the connection of the model systems with real polymer solutions has yet to be improved.<sup>[20]</sup> Close comparisons between the predictions of models and the results of experiments is necessary to verify

the codes and to receive scaling laws for the polymer-flow interaction. A full model of turbulent pipe flow interacting with polymer molecules to precisely predict drag reduction of real polymers has not been achieved yet. Therefore, it is important to provide studies of the behaviour of polymeric drag reducing agents in systems, that closely resemble industrial applications, as long as the influence of different parameters like flow geometry and polymer-solvent interaction is not fully understood and scaling of the polymer-flow interaction is not available.

A major challenge in long term applications such as pipelines is the degradation of polymeric drag reducing agents. When in use, the molecular weight and the drag reduction capability of the dissolved polymers decrease. The degradation has been encountered for different drag reduction systems and empirical models have been established in order to explain and predict the effect,<sup>[21]</sup> some with theoretical implications.<sup>[10, 22, 23]</sup> Albeit broadly accepted they are not verified for technical applications in pipe-flow. So, it is of particular interest to study the behaviour of polymeric drag reducing agents in large pipe-flow systems. This ensures the connection between models and previous studies with applications in industry.

## 1.2 Project aim: Long term characterisation of DRAs in pipe-flow

The aim of this work was to investigate the long-term behaviour of a polymeric drag reducing agent in a pilot scale pipe-flow system at high Reynolds numbers. The facility used was originally designed by Zadrazil.<sup>[14]</sup> Polymer solutions flow through a 7.2 m long test section with Reynolds numbers up to  $10^6$ ; cyclic operation enables the simulation of flow-paths with a length scale of kilometres. It operates with pressure driven flow, in order to avoid the incorporation of a pump into the flow-path, so the polymer degradation is expected to be mainly caused by shear forces in turbulent pipe flow. Further description of the flow facility can be found in section 2.2.

In order to provide a comprehensive picture of the behaviour of polymeric drag reduction agents, additional methods were used to characterize the polymers and the solutions. Samples from the repeatedly pumped solutions were taken at different stages of the experiment. By gel permeation chromatography (GPC) and rheometry their molecular weight and their flow behaviour in Couette and Taylor flow were investigated. This enabled a direct link of changes in drag reduction and changes in molecular properties.

### 1.3 Theoretical background

#### 1.3.1 Fluids in pipes

The Reynolds number (Re) is a dimensionless parameter that describes the nature of the flow of a fluid, characterizing the transition from laminar to turbulent flow. It is defined as the ratio of the inertial forces to the viscous forces present in the fluid. In pipe flow, Re is calculated as the product of the density of the fluid  $\rho$ , the mean flow velocity  $U$  and the pipe diameter  $d$ , divided by the dynamic viscosity of the fluid  $\eta$  (Equation 1.1). Reynolds described how above a certain value of this ratio, turbulence appeared in pipe-flow and below a certain value it transitioned back into laminar flow.<sup>[24]</sup>

$$\text{Re} = \frac{\rho d U}{\eta} \quad \text{Equation 1.1}$$

The frictional resistance a fluid encounters in a pipe is expressed by the Fanning friction factor  $f$  (equation 1.2). It is defined as the pressure drop  $\Delta p$  over a certain distance  $l$  for a given pipe diameter, fluid density and flow velocity. The pressure drop is the difference in pressure before and after the pipe.

$$f = \frac{\Delta p}{l} \frac{d}{2 \rho U^2} \quad \text{Equation 1.2}$$

As long as the flow is laminar, the behaviour of a Newtonian fluid follows Poiseuille's law (equation 1.3).<sup>[2]</sup> After the transition to turbulent flow, it can be described by the empirical Prandtl-von-Kármán law (equation 1.4).<sup>[2]</sup> When expressed in Prandtl-von-Kármán coordinates,  $f^{-0.5}$  vs.  $\log_{10}(\text{Re} \sqrt{f})$ , the behaviour in turbulent flow is linear (Fig. 1.1).

$$\frac{1}{\sqrt{f}} = \frac{\text{Re} \sqrt{f}}{16} \quad \text{Equation 1.3}$$

$$\frac{1}{\sqrt{f}} = 4.0 \log_{10}(\text{Re} \sqrt{f} - 0.4) \quad \text{Equation 1.4}$$

$$\frac{1}{\sqrt{f}} = 19.0 \log_{10}(\text{Re} \sqrt{f} - 32.4) \quad \text{Equation 1.5}$$

If drag reducing agents are added to the liquid, its behaviour in turbulent flow deviates from the Prandtl-von-Kármán law. The deviation occurs only above a certain threshold of  $Re$  which is called the onset point of drag reduction.<sup>[2]</sup> At larger  $Re$ , the reduced pressure drop causes a decreased friction factor (increased  $f^{-0.5}$ ). This drag reduction depends on the polymer, its concentration, the solvent and the geometry of the system. The deviation from the Prandtl-von-Kármán increases with  $Re$ . However, the maximum drag reduction that can be achieved at a given Reynolds number is independent of those parameters. It is described by Virk's asymptote for maximum drag reduction (Equation 1.5).<sup>[25]</sup> Experimental results taken from [2] are shown in Fig. 1.1. The friction factors of different drag reduction systems determined in gross flow measurements are plotted in Prandtl-von-Kármán coordinates. In laminar flow they follow Poiseuille's law. After the onset point of drag reduction  $f$  is smaller than in the turbulent flow of the pure solvent. With increasing  $Re$  all solutions of drag reducing agents converge to Virk's asymptote.

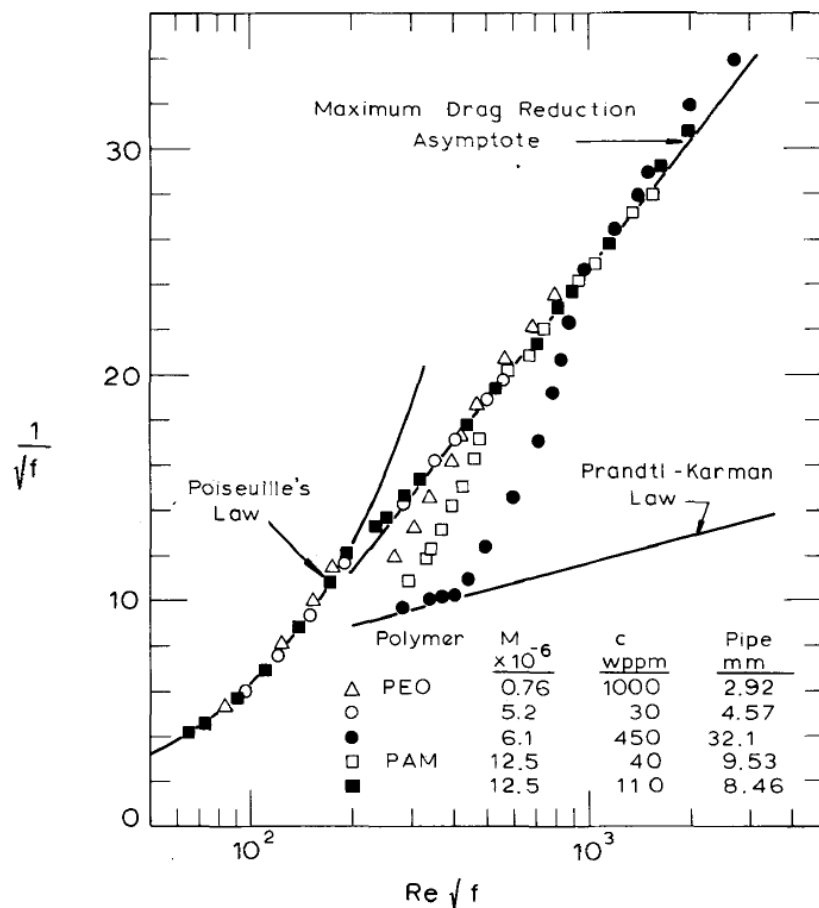


Figure 1.1: Fanning friction factor of polymer solutions in laminar and turbulent pipe-flow, taken from [2]. At low  $Re$ , the solutions follow Poiseuille's law for laminar flow. At higher  $Re$  their behaviour differs from the Prandtl-von-Kármán law for turbulent fluids, causing drag reduction.

### 1.3.2 Drag reduction in turbulent pipe flow

Drag reduction (DR) can be defined as difference of the Fanning friction factor of the pure solvent  $f_s$  and of the friction factor of the polymer solution  $f$  relative to the factor of the pure solvent at a constant Re (Equation 1.6).<sup>[26]</sup> With this definition the drag reduction describes how much the frictional resistance of a given flow is reduced by the addition of a drag reducing agent.

$$DR = \left( \frac{f_s - f}{f_s} \right)_{Re} \quad \text{Equation 1.6}$$

If the mass density and the viscosity are the same for the pure solvent and the solution, the drag reduction can be calculated from the difference in pressure drops along the pipes only (Equation 1.7).

$$DR = \left( \frac{\Delta p_s - \Delta p}{\Delta p_s} \right)_{Re, \rho, \eta} \quad \text{Equation 1.7}$$

### 1.3.3 Degradation of polymeric drag reducing agents

Polymer degradation in flow results in a decreased drag reduction.<sup>[27]</sup> In turbulent flow the polymer chains are broken by the shear forces, causing their drag reducing capability to be lowered. Brostow developed a model to describe this mechanical degradation and compared it to experimental results of other authors.<sup>[23]</sup> He derived a decay function which should be valid for all drag reduction systems (Equation 1.8). In this equation, the drag reduction DR and mean molecular weight  $M$  of a polymer relative to the properties at the start of the experiment ( $t = 0$ ) decrease with time, depending on a rate constant  $h_0$ . The model assumes an end in polymer degradation, leaving a drag reduction  $> 0$  at  $t = \infty$ . Its value is governed by the number of weak points in the polymer chain  $W$ . After the molecule has broken into  $W+1$  pieces further chain scission becomes unlikely.

$$\frac{DR}{DR_{t=0}} = \frac{M}{M_{t=0}} = \frac{1}{1 + W (1 - e^{-h_0 t})} \quad \text{Equation 1.8}$$

The independent coordinate chosen in Brostow's model is the time that the polymer is exposed to mechanical stress  $t$ . In pipe-flow facilities, operating with a constant flow velocity, this time is directly proportional to the distance the solution travels through the pipe. Some previous studies on polymer degradation in cyclically operated pipe-flow facilities used the number of runs the polymer solution

was recirculated.<sup>[12, 21]</sup> Depending on the duration of a run and the dimensions of the facility, the number of runs is proportional to the travelling time.

### 1.3.4 Behaviour of fluids in Couette-Taylor-flow

The behaviour of a fluid sheared between rotating concentric cylinders, e.g. a rheometer equipped with a double gap geometry, differs from the flow in a pipe. Instead of just laminar and turbulent flow multiple different flow regimes can be distinguished. For small Reynolds numbers a purely azimuthal Couette-flow arises. No vortices are present and for a Newtonian fluid the encountered shear stress  $\tau$  is the product of the shear rate  $\dot{\gamma}$  and the constant viscosity. In the other regimes, occurring at enhanced shear rates, the viscosity changes with the shear rate; this apparent shear viscosity  $\dot{\eta}$  is defined by Equation 1.9.

$$\dot{\eta} = \frac{\tau}{\dot{\gamma}} \tag{Equation 1.9}$$

If the shear rate is increased (corresponding to an increase in Re) the Couette-flow will transform into Taylor-flow. Taylor vortices are formed perpendicular to the azimuthal flow. In contrast to turbulent flow, Taylor-flow is still steady and the vortices are well defined. At even higher shear rates the flow

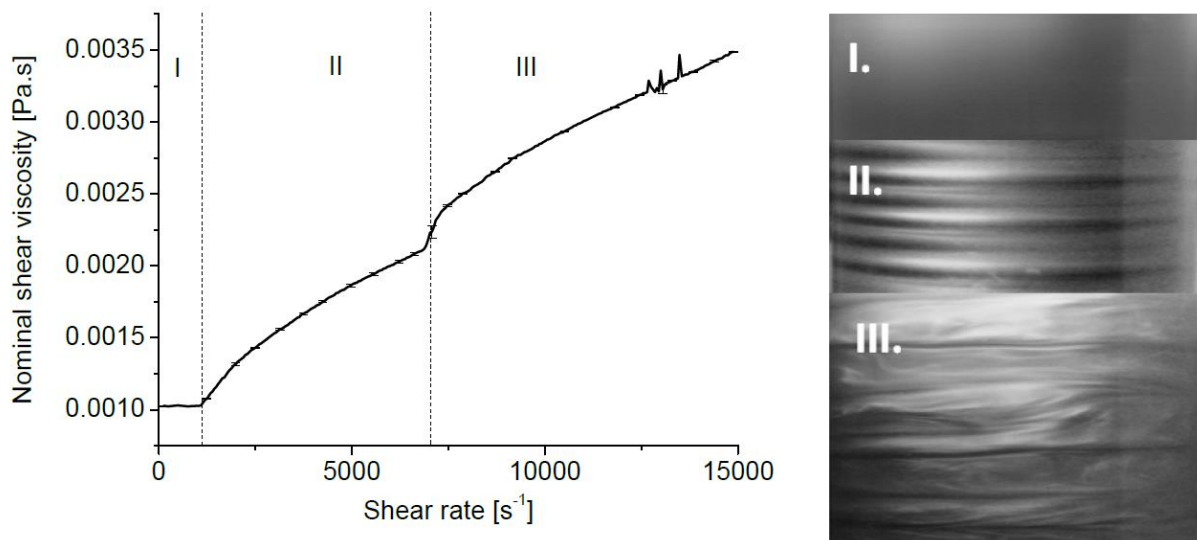


Figure 1.2: Viscosity of pure water, estimated by Zadrazil.<sup>[14]</sup> The onset points of the different regimes are indicated. I: Couette-flow, II: Taylor-flow and III: turbulent Taylor-flow. The pictures of the rotating fluid show the different flow patterns.

will change into fully chaotic turbulent flow. Both transitions cause an abrupt rise in the apparent shear viscosity. A viscosity profile of water and pictures of the flow pattern (both taken from [14]) are shown in Fig. 1.2. Studies have pointed out that it is possible to estimate the drag reduction capability of a polymer from its behaviour in Taylor-flow.<sup>[28]</sup>

### 1.3.5 Characteristics of the molecular weight distribution of polymers

Synthetic polymers show a size distribution; the molecules do not have a uniform molecular weight. Instead, the chain length of the molecules is distributed over an interval. The properties of the polymer depend on the mean molecular weight as well as width and shape of the distribution. The main characteristics are the weight average molecular weight  $M_w$ , the number average molecular weight  $M_n$ , the viscosity average molecular weight  $M_\eta$  and the molar mass dispersity  $\mathcal{D}_M$ . Their definitions are listed as Equation 1.10, 1.11, 1.12 and 1.13.

$$M_w = \frac{\sum N_i M_i^2}{\sum N_i M_i} \quad \text{Equation 1.10}$$

$$M_n = \frac{\sum N_i M_i}{\sum N_i} \quad \text{Equation 1.11}$$

$$M_\eta = \left( \frac{\sum N_i M_i^{1+\alpha}}{\sum N_i M_i} \right)^{\frac{1}{\alpha}} \quad \text{Equation 1.12}$$

$$\mathcal{D}_M = \frac{M_w}{M_n} \quad \text{Equation 1.13}$$

All averages provide information of the chain-length of the polymer molecules.  $M_n$  is the arithmetic mean of the weight of all molecules, with  $N_i$  being the number of molecules in each weight fraction and  $M_i$  their molecular weight. In  $M_w$  the contribution of each fraction is additionally weighted by its molecular weight.  $M_\eta$  is the molecular mass determined by viscosity measurements. It uses the Mark-Houwink parameter  $\alpha$ , which depends on the polymer solvent system and on the temperature. Compared with  $M_n$ ,  $M_w$  is less influenced by errors in the estimation of the weight of small molecules. The ratio of the two is  $\mathcal{D}_M$ . It indicates the broadness of the distribution. If the size of the molecules is distributed over a broad interval,  $M_n$  is much smaller than  $M_w$ .

### 1.3.6 Gel Permeation Chromatography

The molecular weight distribution of a polymer can be analysed in detail using gel permeation chromatography (GPC). In a GPC column the molecules are separated according to their hydrodynamic radius which depends on the molecular weight. The column is filled with a porous, immobilized material with non-uniform pore size. The polymer molecules diffuse into the pores. The smaller a molecule is, the more pores are available it can enter, causing longer retention times for lower molecular weight. Molecules bigger than the largest pores just flow through the column. This causes an upper exclusion limit of a GPC column.

After elution, different detectors are employed to continuously measure the properties of the solution. Due to the separation different weight fractions are analysed individually:

- A refractometer is used to estimate the difference in refractive index between polymer solution and pure eluent. This difference is directly proportional to the mass concentration of the polymer and to the refractive index increment ( $dn/dc$ ). Because the increment is over a wide range independent of the molecular mass, the refractometer is used as a concentration detector.
- A light scattering detector measures the intensity of light which is scattered by the polymer solution at different angles. At low angles, the intensity is directly proportional to the product of mass concentration and molecular weight of a polymer in solution.
- A differential viscometer is used to measure the viscosity of the polymer solution.

Combining refractive index and light scattering and taking the flow time between the detectors into account, the molecular mass of each weight fraction can be calculated. This enables the estimation of the average molecular weight and the molar mass dispersity. Calibration standards with known mass distribution are needed in order to account for an instrument sensitivity constant. Taking random peak broadening into account, the weight distribution of the polymer is to some extent resembled by the chromatogram detected by the refractometer.

## 1.4 Properties of polyethylene oxide

The drag reducing agent used in this study was polyethylene oxide (PEO, also known as PEG, polyethylene glycol). PEO is a non-toxic, water-soluble polyether. It was chosen because the results can be linked to a large number of previous studies on the drag reducing capability of this polymer and it is easy to handle. The basic molecular structure of PEO is shown in Fig. 1.3. The polymer is non-ionic, but due to the oxygen atoms incorporated in the backbone, it interacts well with polar solvents.

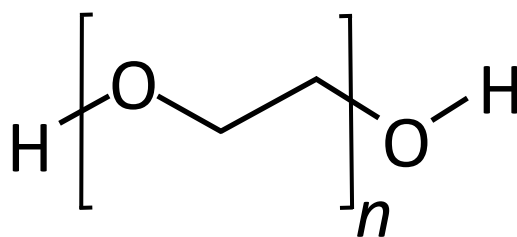


Figure 1.3: Chemical structure of polyethylene oxide. The polymer is soluble in polar solvents, due to the high number of oxygen atoms incorporated in the chain.

High drag reducing capability of PEO has been reported,<sup>[2]</sup> but there is some disagreement about its long-term behaviour and the role of aggregates.<sup>[29]</sup> In an aggregate, multiple molecules are stuck together by non-covalent bonds. Studies have shown their spontaneous formation even in dilute solutions of PEO.<sup>[30]</sup> Changes in drag reduction are linked to the breakup of aggregates in turbulent flow. A more common model for changes in DR is the breakup of covalent bonds and the scission of the polymer backbone.<sup>[16]</sup> Aggregation and chain scission can already happen during the preparation of the solution, depending on the procedure and the molecular weight of the polymer.<sup>[29]</sup> Even in quiescent conditions a decrease in the molecular weight of dissolved PEO has been found, happening on a timescale of days.<sup>[31]</sup> It is important to take this behaviour into account when performing long term drag reduction experiments.

## 2. Experimental Methods

### 2.1 Materials

The polyethylene oxide (PEO) used in this study was purchased from Sigma Aldrich. Two samples with different molecular weights were used. According to the manufacturer they had viscosity average molecular weights of  $4 \cdot 10^6$  g/mol and  $2 \cdot 10^5$  g/mol. The polymers were dissolved in tap water from the First Vienna Mountain Spring Pipeline, taken between October and December 2019. It was used without further purification. The two polymer solutions were called 4E6 and 2E5, referring to the molecular weights stated by the manufacturer.

For the GPC system an eluent containing 0.1 mol/L  $\text{NaNO}_3$  and 200 wppm  $\text{NaN}_3$  in deionized water was used.  $\text{NaNO}_3$  and  $\text{NaN}_3$  were purchased from Sigma Aldrich. Prior use, the solution was filtered through a 0.2  $\mu\text{m}$  nylon filter. In order to calibrate the GPC-system, PEO standards provided by Agilent EasiVials were used. Information about the calibration standards can be found in Appendix A.

All deionized water used in this study was produced by an ELGA PURELAB Classic system and had a conductivity of 0.055  $\mu\text{S}$ .

### 2.2 Drag reduction measurements in a pipe flow facility

The behaviour of PEO used as a drag reducing agents was studied using a flow facility originally designed by Zadrazil<sup>[14]</sup> and modified at the University of Vienna. The current setup is called Vienna Experiment for Drag Reducing Agents (ViEDRA). A schematic is given in Fig. 2.1 and a picture in Fig. 2.2. The polymer solution was prepared in the mixing tank (tank I) using an impeller. From the mixing tank, it flowed into the pressure tank (tank II) through a valve (V2) driven by gravity. Valve 1, 2, 3 and 5 were regulated pneumatically, allowing for automated control by the software. Two valves (V4 and V6) were operated manually. They were used only for cleaning the system. The section between valve 2 and valve 5 could be pressurized by applying compressed air from an external network (nominal pressure of the compressed air: 7 bar). Valve 1 and 3 were used to control the pressure in the tank. The tank was equipped with a pressure and level sensor. From the pressure tank the solution passed a magneto-inductive flowmeter (Sitrans F M Magflo MAG5000, Siemens, Denmark) and a flow straightening device (honeycomb). It then passed the test section which was equipped with differential pressure transducers (Deltabar S, Endress+Hauser, Germany) to measure the pressure drop over six different distances. The test section was a 7.2 m long straight stainless-steel pipe with an inner diameter of 26 mm and one welding only. The reference point of the pressure transducers was located 1.76 m into

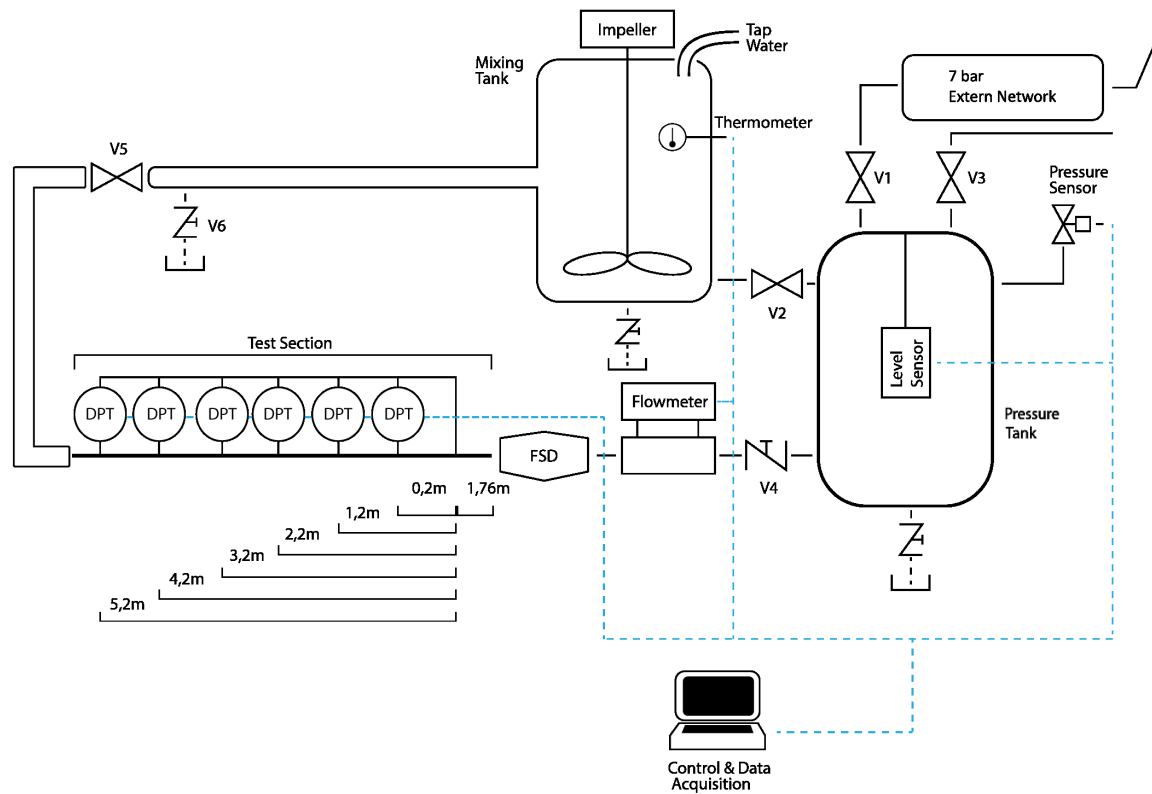


Figure 2.1: Schematic representation of VIEDRA. During one run the solution flowed pressure driven from the pressure tank through a flowmeter, a flow straightening device and the test section into the mixing tank while the temperature, the flow rate and the pressure drop along the test section were monitored.

the test section and the differential pressures were measured over distances of 0.2, 1.2, 2.2, 3.2, 4.2 and 5.2 m. Behind the test section the solution was returned to the mixing tank through a 10.5 m long plastic tube with an inner diameter of 30 mm. The total distance the solution travelled in one run was roughly estimated to be 19.6 m of pipes, tubes and tanks.

During the flow experiment the solution was characterised by its temperature (measured in tank I), the flowrate (measured by the flowmeter) and the pressure drop along the test section. The flow was pressure driven. The control software kept the Reynolds number within  $\pm 5\%$  constant during each run by adjusting the pressure applied in tank II and taking the gravity contribution of the water in the tank into account. For each run mean values of the pressure drop and the flowrate were calculated. 1/3 of the data points at the start and at the end of each run were excluded, because the system had not reached a constant flowrate. Slight changes were found in the flowrates estimated by the flowmeter on different days. The volume measured by the level-sensor in the pressure tank was used to correct the results of the flowmeter: The flowrate was divided by the ratio of the volume changes measured with the level sensor and the flowmeter during the day it was measured and multiplied by the ratio of

the volume changes measured with the level sensor and the flowmeter during the day of the reference measurements. This ensured that the flowmeter results of the sample and the reference had no error relative to each other and that the pressure drop of the solution of DRAs was compared to a reference value with the same  $Re$ .

From the measured quantities the Reynolds number, the fanning friction factor and the drag reduction were calculated. The temperature dependent dynamic viscosity and density of deionized water were taken from [32]. The apparent viscosity of samples of the polymer solution was estimated (see section 3.3), but the measurement temperature differed from the temperature of the solution in ViEDRA. For the majority of runs, the influence of the temperature on the viscosity was stronger than the influence of the polymer. So, the viscosity of water was used to calculate the properties in all runs.

Long-term cyclic operation allowed to simulate pipelines with a length scale of kilometres. At the end of each run the solution was collected in the mixing tank. By driving the same solution of drag reducing agents through the test section repeatedly, the long-term behaviour of PEO was investigated. The change in drag reduction was continuously monitored and samples of the solution were taken after different runtimes. By analysing these samples in a GPC-system, changes in drag reduction were linked to changes in molecular weight.



Figure 2.2: Photos of the Vienna Experiment for Drag Reducing Agents.

### 2.3 Measurements of apparent viscosity in a rheometer

In order to get detailed profiles of  $\dot{\eta}$  versus  $\dot{\gamma}$  for Couette- and Taylor-flow a DHR2 rheometer (TA Instruments) was used. It was equipped with a double gap geometry with the following dimensions (Fig. 2.3): Double wall concentric cylinders, inside cup diameter 30.2 mm, inside bob diameter 32.03 mm, outside bob diameter 34.99 mm, outside cup diameter 37 mm, inner cylinder height 55 mm, immersed height 53 mm, geometry gap 2 mm.

For each sample, the same procedure was executed: 12 mL were filtered (0.45  $\mu\text{m}$  nylon filters) and filled into the geometry. The solution was pre-sheared at a shear rate of  $100 \text{ s}^{-1}$  for 1 min, then a ramp was performed, increasing the shear rate from  $100 \text{ s}^{-1}$  to  $300 \text{ s}^{-1}$  over the course of 3 min and finally the shear-rate was increased stepwise. The shear rate was increased from  $100 \text{ s}^{-1}$  to  $205 \text{ s}^{-1}$  in steps of 1 to  $5 \text{ s}^{-1}$ , holding each shear rate for 10 s and data sampling with a frequency of 1 Hz while the temperature of the solution was kept at  $25.00^\circ\text{C}$ . For the samples of pure tap water and deionized water the stepwise increase was extended to a range from  $30 \text{ s}^{-1}$  to  $1000 \text{ s}^{-1}$  but with a larger step size. The apparent viscosity measured with the stepwise method were used to determine the viscosity in Couette-flow and the onset point of Taylor flow.

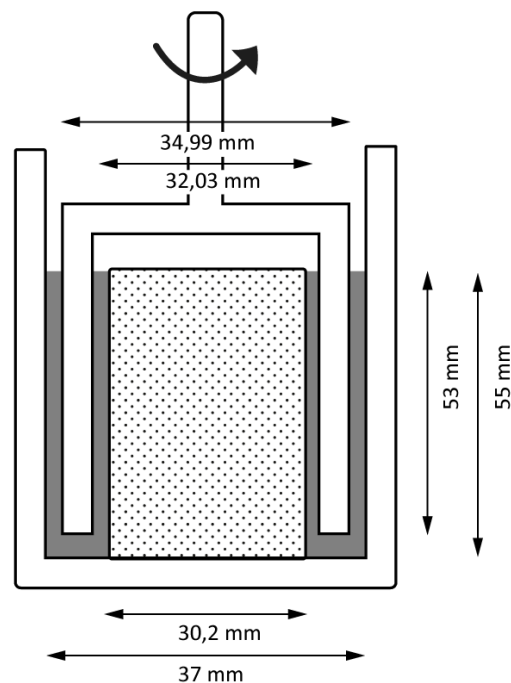
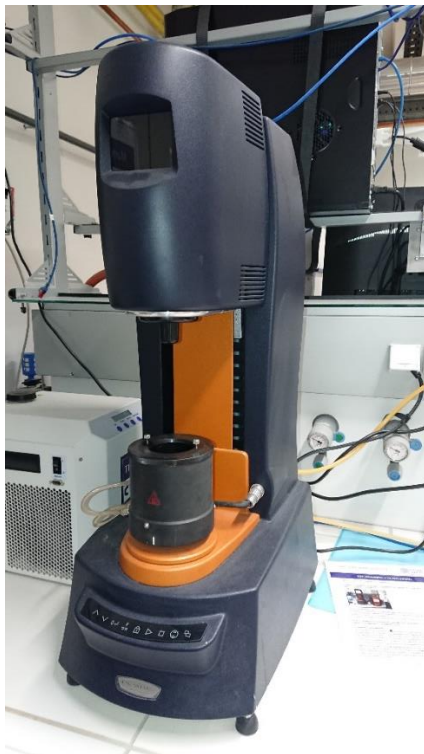


Figure 2.3: DHR2 rheometer (TA Instruments) equipped with a double gap geometry used for measuring viscosity profiles.

## 2.4 Execution of molecular weight measurements using GPC

The GPC setup used consisted of a solvent reservoir, a degasser (CSI6150 4 channel degasser, laserchrom), an HPLC pump (LC-20 ADVP, SHIMADZU DEUTSCHLAND GmbH), an automatic sample injector (S5200 Sykam GmbH) and a triple detection GPC-system (Viscotec TDA 302, Malvern Panalytic). A 0.2  $\mu\text{m}$  nylon filter, the columns (guard column, analytical columns A4000, exclusion limit  $1 \cdot 10^6$  g/mol and A6000M, exclusion limit  $20 \cdot 10^6$  g/mol) and the detectors (low angle light scattering (LALS), right angle light scattering (RALS), refractive index (RI), differential viscosimeter (VIS)) were situated in an oven, kept at a constant temperature of 30°C. A schematic representation is given in Fig. 2.4 and a picture of the setup is shown in Fig. 2.5.

During the measurements, the eluent (0.1 mol/L  $\text{NaNO}_3$  and 200 wppm  $\text{NaN}_3$  in deionized water) was pumped with a constant flowrate of 0.7 mL/min. Each sample was filtered through a 0.45  $\mu\text{m}$  nylon filter before it was injected into the flow. Depending on the sample, different analytical columns were used (A4000, A6000M or both).

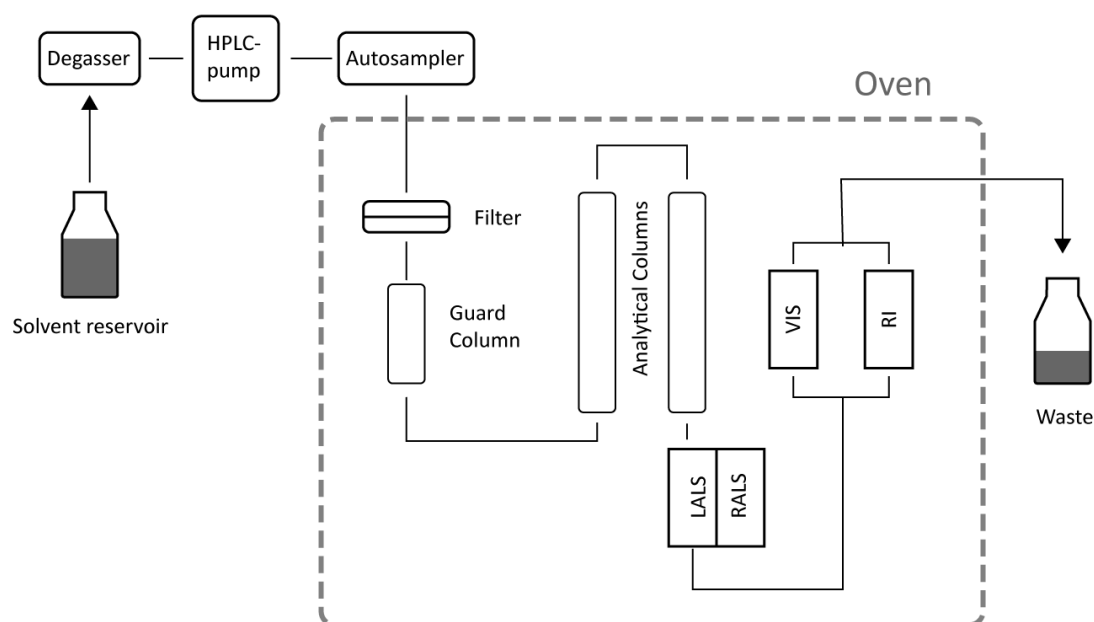


Figure 2.4: Schematic representation of the GPC setup used. Polymer molecules in the sample were separated in the analytical columns and their properties were analysed in the detectors thereafter.



Figure 2.5: Photograph of the GPC setup.

## 2.5 Experiments performed

### 2.5.1 Reference measurements

To receive reference values of the pressure drop of the pure solvent in the test section 248 L tap water were filled into ViEDRA and runs with varying Reynolds numbers were performed. In total 39 runs with  $Re$  in the range of  $3.3 \cdot 10^4$  to  $10.8 \cdot 10^4$  were carried out. The results of five runs had been excluded, because the measured parameters were not stable over the course of the run. Pressure drops versus  $Re$  of 12 runs with  $Re$  between  $9.0 \cdot 10^4$  and  $10.8 \cdot 10^4$  were fitted by a parabola for each pressure transducer. These fits were used to calculate the reference pressure drops for the ViEDRA runs with polymer solutions, which had Reynolds numbers between  $9.6 \cdot 10^4$  and  $10.5 \cdot 10^4$ .

The apparent viscosity of tap and deionized water was measured at different shear rates.

The GPC-system was calibrated with PEO-standards. The standards were dissolved in deionized water and measured. For the results and the calibration see appendix A.

### 2.5.2 Solutions of polyethylene oxide

For PEO with  $M_n = 4 \cdot 10^6$  g/mol a solution containing 100 wppm polymer in tap-water was prepared in the mixing tank of ViEDRA (4E6). The polymer powder was added to 300 L tap water over the course of 30 min while stirring to avoid macroscopic aggregation. Afterwards the polymer was allowed to dissolve undisturbed for 24 h. During the next days, samples of the solution in the mixing tank were taken (50 mL each) and runs of ViEDRA were performed. All runs had Reynolds numbers between  $9.6 \cdot 10^4$  and  $10.5 \cdot 10^4$ . For each run the drag reduction was calculated, using the pressure drop of the reference measurements at the same Reynolds number.

The samples taken during the long-term experiment were analysed via GPC and rheometry. This allowed us to link the drag reducing properties of the solution to the properties of the polymer molecules. The molecules of the different samples travelled a certain distance through ViEDRA. In addition, the GPC analysis of several samples was repeated several times after 1 to 100 days in order to quantify ageing of the polymer solutions (noted as multiple measurement dates in Table 2.2). This was necessary because the experiment was performed over several weeks and for some samples the first GPC measurement was performed several days after it was taken from the flow facility (see Table 2.2). The repeated measurements enabled us to determine the molecular weight at the day the sample had been taken and to distinguish between aging and degradation in the long-term experiment (see 3.5: Untangling ageing and degradation).

Due to evaporation and leakage the total amount of liquid in the flow facility changed over the course of the experiment. In addition polymer solution was spilled during the 170<sup>th</sup> run. Due to an error in the control measurements the pressure tank ran dry and air was blown through the test section. The tube after V5 disconnected from the mixing tank and about 10 L were spilled. The total amount of liquid was measured during the preparation of the solution and after the experiment had finished.

A second solution containing 100 wppm PEO with  $M_n = 2 \cdot 10^5$  g/mol (2E5) was prepared and analysed the same way. Table 2.1 lists basic information of both long-term experiments. Information about the samples that were taken between the runs is shown in Table 2.2. It is noted if the sample was also characterized in the rheometer and which GPC-columns were used to separate the polymer (a: A4000, b: A6000M, a+b: both).

Table 2.1: Basic information about the long term drag reduction experiments

DRA	$V_{(start)}$ [L]	$V_{(end)}$ [L]	$m_{PEO}$ [g]	$c_{(start)}$ [wppm]	number of runs	total samples	timeframe of DR experiment [d]	timeframe of ageing experiment [d]
4E6	346	258	34.45	100	1333	39	28	100
2E5	291	291	28.91	100	130	6	2	-

Table 2.2: Samples taken from ViEDRA

DRA	sample denomination	number of runs	age at the day of sampling [d]	rheological characterised	age at the day of the GPC experiment [d]
4E6	V1	0	1	yes	1 <sup>b</sup> , 3 <sup>b</sup> , 63 <sup>a+b</sup>
	V2	1	1	yes	1 <sup>b</sup> , 3 <sup>b</sup> , 10 <sup>b</sup> , 15 <sup>b</sup> , 21 <sup>b</sup> , 24 <sup>b</sup> , 63 <sup>a+b</sup> , 100 <sup>a+b</sup>
	V3	5	1	yes	1 <sup>b</sup> , 3 <sup>b</sup>
	V4	15	1	yes	1 <sup>b</sup> , 3 <sup>b</sup> , 10 <sup>b</sup> , 21 <sup>b</sup> , 63 <sup>a+b</sup> , 100 <sup>a+b</sup>
	V5	35	2	yes	1 <sup>b</sup> , 3 <sup>b</sup>
	V6	40	2	yes	3 <sup>b</sup> , 10 <sup>b</sup> , 63 <sup>a+b</sup>
	V7	75	2	yes	3 <sup>b</sup> , 10 <sup>b</sup>
	V8	120	2	yes	3 <sup>b</sup> , 10 <sup>b</sup> , 21 <sup>b</sup> , 63 <sup>a+b</sup>
	V9	120	3	yes	3 <sup>b</sup> , 10 <sup>b</sup>
	V10	150	3	yes	3 <sup>b</sup> , 10 <sup>b</sup> , 21 <sup>b</sup>
	V11	173	7	yes	10 <sup>b</sup>
	V12	205	7	yes	10 <sup>b</sup>
	V13	205	8	yes	10 <sup>b</sup>
	V14	245	8	yes	10 <sup>b</sup> , 15 <sup>b</sup> , 63 <sup>b</sup>
	V15	245	9	yes	10 <sup>b</sup>
	V16	300	9	yes	10 <sup>b</sup>
	V17	300	10	yes	10 <sup>b</sup>
	V18	332	10	yes	10 <sup>b</sup> , 15 <sup>b</sup> , 21 <sup>b</sup> , 63 <sup>b</sup> , 100 <sup>a+b</sup>
	V19	341	11	yes	15 <sup>b</sup>
	V20	400	11	yes	15 <sup>b</sup>
	V21	400	14	yes	15 <sup>b</sup> , 63 <sup>a+b</sup>
	V22	444	14	yes	15 <sup>b</sup> , 21 <sup>b</sup> , 24 <sup>a+b</sup>
	V23	444	15	yes	15 <sup>b</sup>
	V24	540	15	yes	15 <sup>b</sup> , 21 <sup>b</sup> , 63 <sup>a+b</sup>
	V25	540	16	yes	21 <sup>b</sup>
	V26	600	16	yes	21 <sup>b</sup>
	V27	650	16	no	21 <sup>b</sup>
	V28	750	17	yes	21 <sup>b</sup>
	V29	806	17	no	21 <sup>b</sup>
	V30	806	18	no	21 <sup>b</sup>
	V31	927	18	yes	21 <sup>b</sup>
	V32	927	21	no	21 <sup>b</sup>
	V33	1000	21	yes	21 <sup>b</sup>
	V34	1018	22	no	24 <sup>b</sup>
	V35	1153	22	no	24 <sup>b</sup>
	V36	1153	23	no	24 <sup>b</sup>
	V37	1227	23	yes	24 <sup>b</sup>
	V38	1228	24	no	24 <sup>b</sup>
	V39	1333	24	yes	24 <sup>b</sup>
2E5	V1_2E5	0	1	yes	1 <sup>a</sup> , 3 <sup>a</sup>
	V2_2E5	5	1	yes	1 <sup>a</sup> , 3 <sup>a</sup>
	V3_2E5	27	1	yes	3 <sup>a</sup>
	V4_2E5	80	1	yes	1 <sup>a</sup> , 3 <sup>a</sup>
	V5_2E5	80	2	no	3 <sup>a</sup>
	V6_2E5	130	2	yes	3 <sup>a</sup>

### 3. Results and Discussion

#### 3.1 Flow characterisation in ViEDRA

Fig. 3.1 gives an overview of the results of gross flow measurements of polymer solutions and water performed using ViEDRA. For the pure solvent  $Re \cdot \sqrt{f}$  was varied by a flowrate scan. The determined Fanning friction factor  $f$  followed closely the Prandtl-von-Kármán law for turbulent Newtonian fluids. For the polymer solutions  $Re$  was kept between  $9.5 \cdot 10^4$  and  $10.5 \cdot 10^4$ . During the experiment, the molecular weight of the polymer (4E6) decreased. Decreasing  $M_w$  resulted in an increasing Fanning friction factor. The solution did not reach Virk's asymptote for maximum drag reduction. Even for the first run of 4E6, with an  $M_w = 2.7 \cdot 10^6$  g/mol, the friction factor of the solution was nearly twice as big as the factor predicted by the asymptote. The results were similar to results of gross flow measurements of PEO-solutions obtained by Zadrazil.<sup>[14]</sup> For shorter chains (2E5 and the last runs of 4E6,  $M_w < 0.5 \cdot 10^6$  g/mol) the flow behaviour of the polymer solutions was like the behaviour of pure tap water.

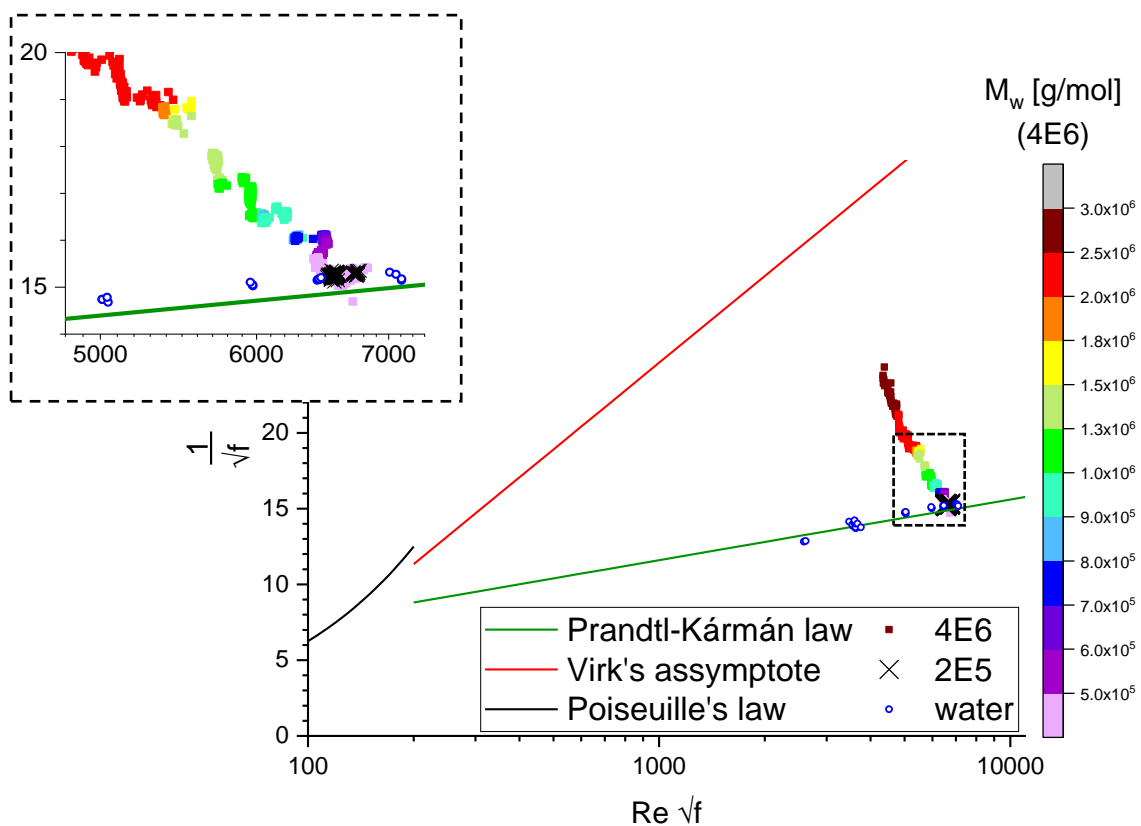


Figure 3.1: Fanning friction factor in Prandtl von Kármán coordinates for the measurements of polymer solutions and tap water. The Fanning friction factor  $f$  increases for polymer solutions with decreasing molecular weight.

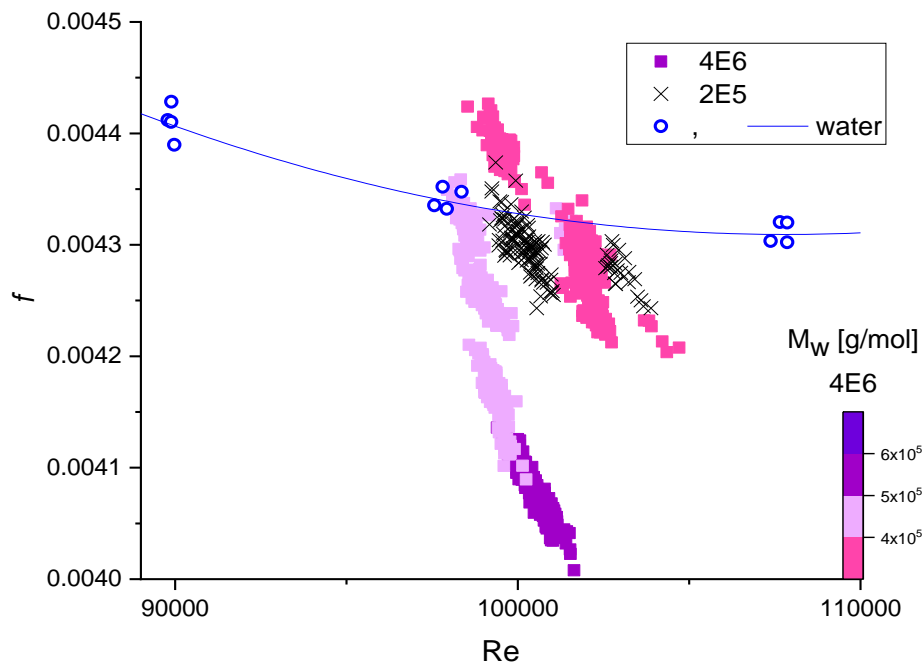


Figure 3.2: Relationship between Fanning friction factor and Reynolds-number; each point corresponds to one run. The slope was different for water and both polymer solutions. The difference in  $f$  and thus the drag reduction depends on  $Re$ . In addition, the curve is shifted depending on the molecular weight of the polymer.

Fig. 3.2 shows the dependency  $f$  on  $Re$ . System intrinsic instabilities caused variations in the flowrate of the polymer solutions. In general  $f$  increased with decreasing molecular weight of the polymer. Due to increased drag reduction at higher  $Re$ , a lower friction factor was measured during some of the last runs of 4E6, even though the polymer had an  $M_w < 4 \cdot 10^5$ .

### 3.2 Drag reduction in long term experiments

The distance the polymer travelled through the flow facility was chosen as the independent variable to study polymer degradation. This reveals how far a drag reducing agent could travel through a pipeline system before it loses its drag reducing capability. To calculate the total distance the polymer travelled through the flow facility after several runs, it is important to take into account that a portion of the solution stayed in the mixing tank and the pressure tank during each run; e.g. if 300 L polymer solution were in the flow facility, 6 runs were performed and in each run 200 L passed through the test section (100 L staying in the mixing tank and in the pressure tank) then the polymer participated on average in 4 runs ( $6 \cdot 200/300$ ).

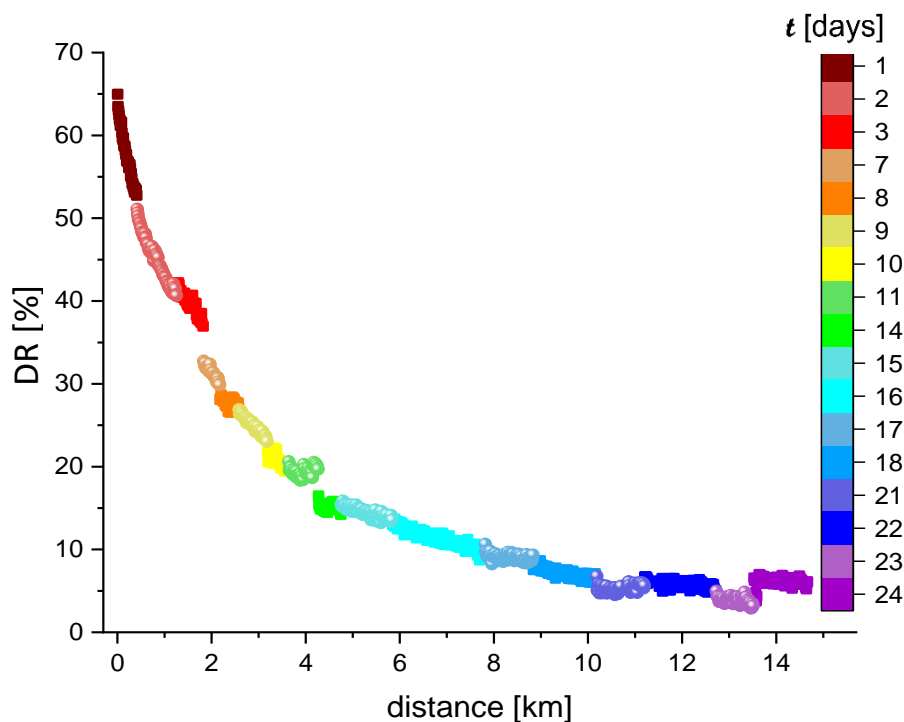


Figure 3.3: Drag reduction over distance of 4E6 (100 wppm),  $Re = 10^5$ . The drag reduction drops during the experiment.

Due to leakage and evaporation the amount of solution decreased during the experiment with 4E6. It was assumed that the total amount of liquid decreased linearly from the volume measured at the start of the experiment to the volume at the end. The volume, that passed the flowmeter during one run was divided by the total amount of liquid in the facility and integrated over all runs. The integrated ratio was multiplied by the length of the flow-path (19.6 m). This gave the distance a polymer molecule travelled on average.

Drag reduction versus distance is plotted in Fig. 3.3, each point corresponding to one run. During the first runs the polyethylene oxide reduced the drag by 65%. The DR capability decreased with the number of runs. After 2 km DR was already halved. It seemed to have reached a lower limit of 5% drag reduction after 10 km, but due to the exponential nature of the decay further experiments would be needed to confirm this (see also Fig. 3.17). After 10 km changes were smaller than deviations caused by day to day variations of measurement parameters. The temperature of the solution varied up to 0.5% and the flowrate up to 8%. In addition, ageing of the polymer solution was detected.

Due to its design and technical problems (hardware and software) the experiment was performed over the course of 24 days. The age of the polymer solution at the time the run was performed is colour coded in Fig. 3.3. At several points changes in measurement day are connected to jumps in drag

reduction. Especially after longer breaks (> 48 h at 2 km and at 4 km), the efficiency of the PEO decreased significantly, despite it had not been sheared. This indicated polymer degradation related to solution ageing on top of the degradation caused by shear forces in the flow.

In Fig. 3.4 the same data set as in Fig. 3.3 is shown, this time the data is coloured according to the Reynolds-number of each run. The ViEDRA control software (feedback control) allows for variations up to 9% in the Reynolds-number. Due to the dependency of the drag reduction on Re some of the scatter can be causally related to those variations. This was especially significant at low drag reduction. A prominent example was the DR-rise at the last experiment day (indicated in Fig. 3.4). Polymer which travelled farther through the flow facility caused higher drag reduction than the polymer measured on the day before because it was measured at a higher Reynolds-number.

Fig. 3.5 shows the DR of 2E5. The drag reduction and the decrease in drag reduction of this polymer solution were similar to the behaviour of 4E6 after it travelled 6 km. However, the slope of the decrease was so small, it was hardly distinct from random scatter. Overall, the shorter polymer produced very little drag reduction.

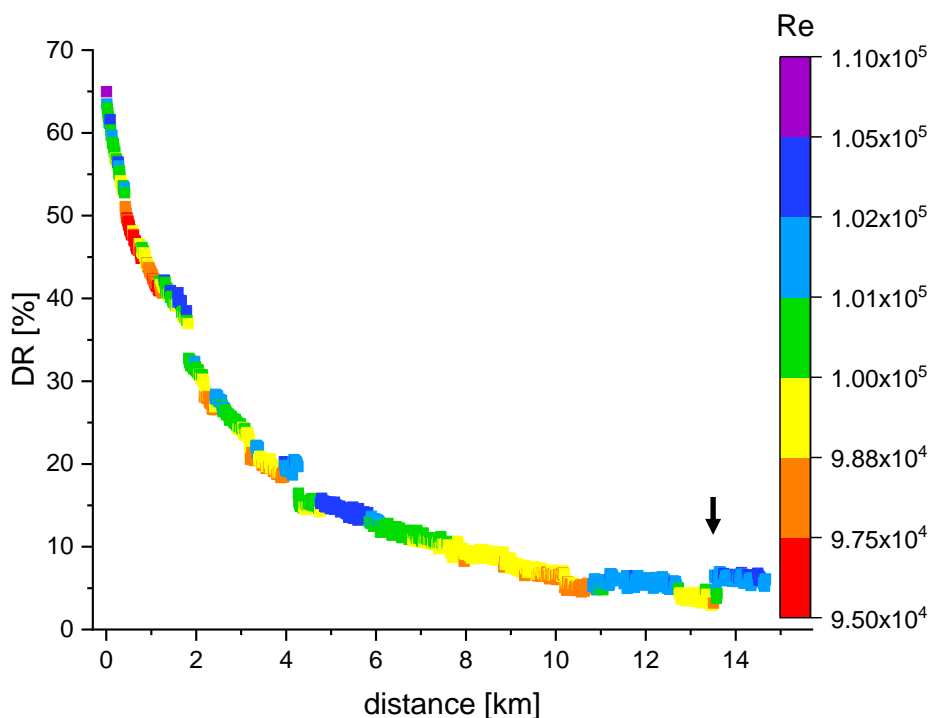


Figure 3.4: Drag reduction of 4E6, coloured by the Reynolds-number of each run. Changes in the Reynolds-number caused variations of the drag reduction, especially for low values. This was the reason for the increased drag reduction at the end of the experiment.

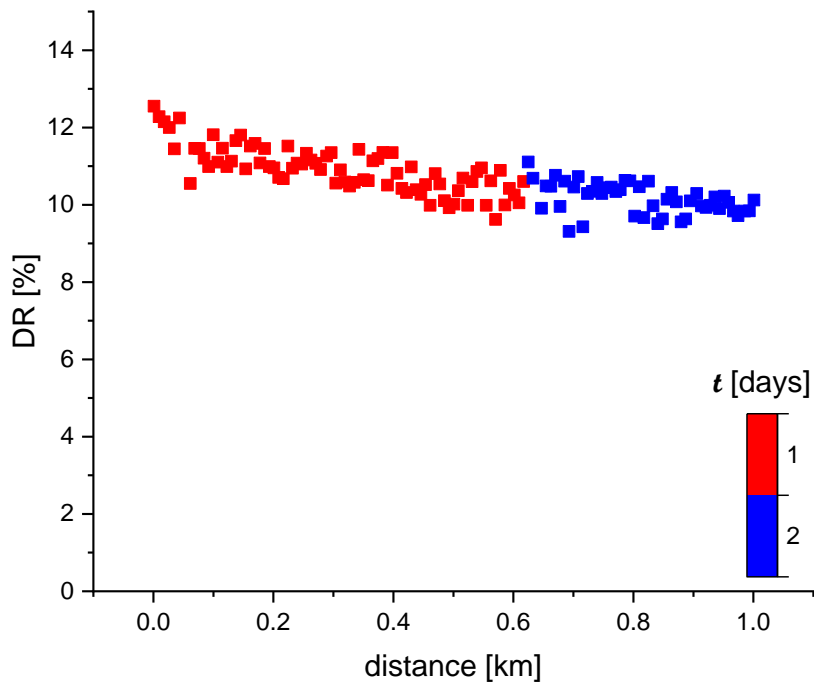


Figure 3.5: Drag reduction of 2E5 (100 wppm),  $Re = 10^5$ . DR decreased slightly over the course of the experiment. The change nearly disappeared in random scatter. Variations in the Reynolds number were below 3%.

### 3.3 Flow characterisation in the Rheometer

Mean values of the viscosity in the Couette-regime are shown in Fig. 3.6. For 4E6 the viscosity changed with the distance the polymer travelled through ViEDRA, indicating changes in molecular weight. After the strong decrease during the first three kilometres the viscosity of 4E6 stayed constant. For 2E5 no systematic trend was visible. It had lower viscosity than the solutions of the polymer with higher  $M_w$ . Tap-water showed behaviour similar to deionized water. Viscosity profiles in Couette- and in Taylor-flow can be found in appendix B.

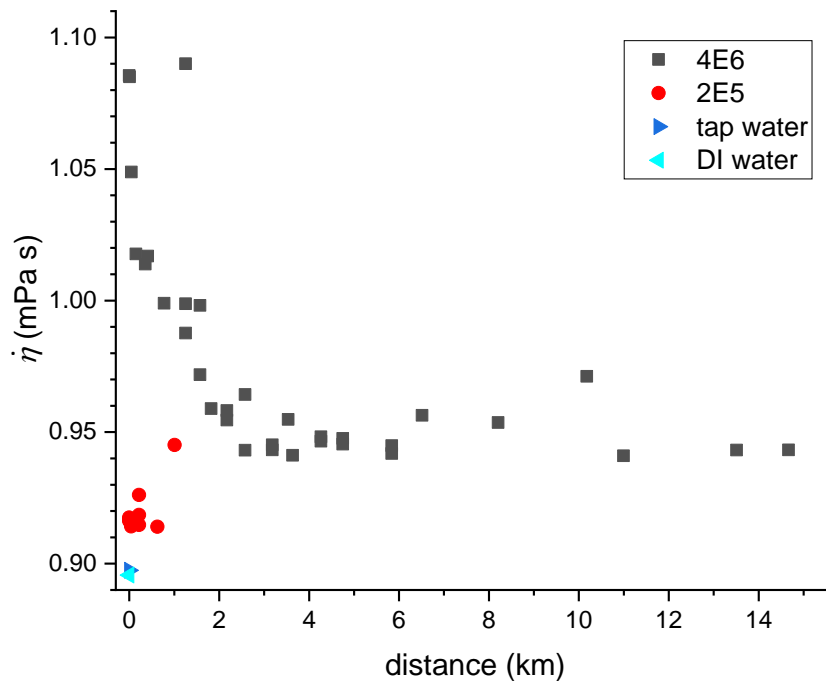


Figure 3.6: Mean viscosity of the solutions in the laminar flow regime. No systematic trend was visible in the viscosity of 2E5. For 4E6 it decreased with the distance the polymers had travelled, but even the last samples had higher viscosities than 2E5.

### 3.4 Molecular weight of sheared polyethylene oxide solutions

The samples taken from ViEDRA were analysed via GPC. Fig. 3.7 shows the weight average molecular weight of each sample of 4E6. The first sample was taken before the first run of ViEDRA. The polymer had an  $M_w$  of  $2.7 \cdot 10^6$  g/mol. Due to shear degradation  $M_w$  decreased below  $0.5 \cdot 10^6$  g/mol after it travelled a distance of more than 8 km. At the same time, the molecular weight of the first sample continued decreasing, while the solution was stored at ambient conditions. After 100 d it was as low as  $1.0 \cdot 10^6$  g/mol. All samples that were measured multiple times showed a similar behaviour.

The samples were not analysed immediately after they were taken from the flow facility. Instead they were collected and measured in groups. This caused steps in Fig. 3.7. In each group the decrease was caused by degradation in shear while differences between the groups were (partly) due to ageing. With ageing  $M_w$  versus distance curves were shifted against each other.

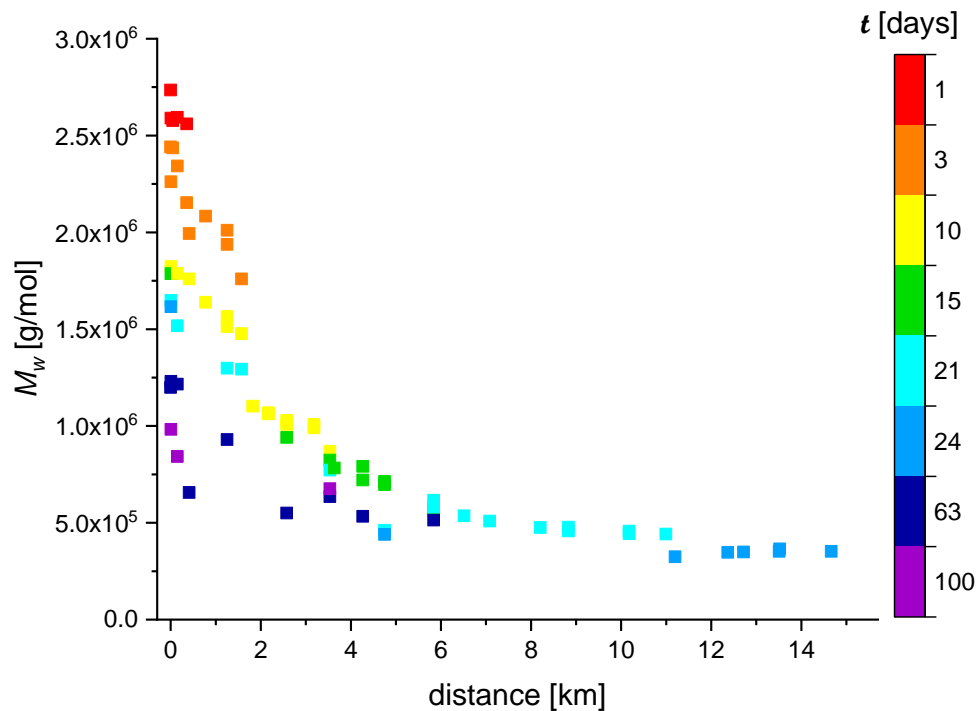


Figure 3.7: The molar weight of 4E6 changed over the course of the experiment. Like the drag reduction, the weight average molecular weight  $M_w$  decreased with increasing travelled distance. Repeated measurements of the same samples confirmed the ageing of the solution.

After 8 km the decrease with distance became less clear. There was a downshift at 11 km, but it was potentially caused by ageing. For  $M_w$  estimated in one group no systematic decrease was found after 8 km.

Fig. 3.8 shows that the molecular weight dispersity increased with time for the samples of 4E6. Except for the measurements during the first day, samples that were measured at the same day had about the same  $\bar{D}_M$ , independent of the distance. This indicates a difference in the mechanism of the degradation due to shear and due to ageing. With time, the mean molecular weight decreased and the weight distribution got broader. Shear forces present in the flow also reduced the mean molecular mass, but changes in  $\bar{D}_M$  were insignificant. For high mass polymers the probability to break in shear flow is greater, which caused reduced broadening of the molecular weight distribution compared to the ageing, which had the same degradation probability for polymers of all lengths.

Calculations have shown that random scission of polymer chains leads to a  $\bar{D}_M$  of 2.<sup>[33]</sup> Experimental results used by Brostow in his study on mechanical degradation gave a value of 1.5 for degraded drag reducing agents. They concluded that the degradation of DRAs is not caused by random Scission.<sup>[23]</sup>

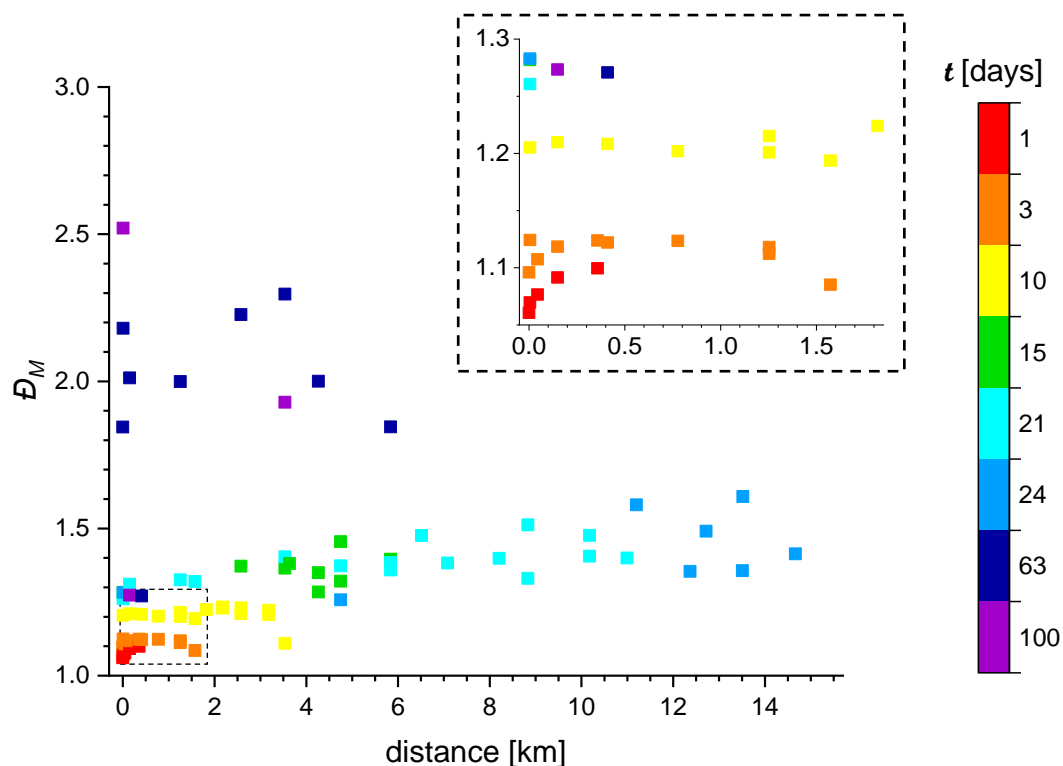


Figure 3.8: The molar weight dispersity of 4E6 increased with the age of the solution. During the first runs it also increased with distance.

For our results, this shows that the ageing could be caused by random scission of the molecules while the degradation in shear is linked to scission at certain points.

For 2E5 the results of the GPC analysis are shown in Fig. 3.9 and Fig. 3.10. The polymer had an  $M_w$  of roughly  $0.9 \cdot 10^5$  g/mol. It remained stable over the course of the experiment.  $M_w$  did not change systematically with time or travelled distance. This is consistent with the observations for 4E6. Even at the end of the experiment 4E6 was at least three times larger than 2E5. For small molecules only very slow degradation is expected, if any at all.  $\mathcal{D}_M$  (Fig. 3.10) of 2E5 indicated a broad molecular weight distribution, which was similar to the distribution of the aged 4E6 samples (age  $\geq 63$  d).

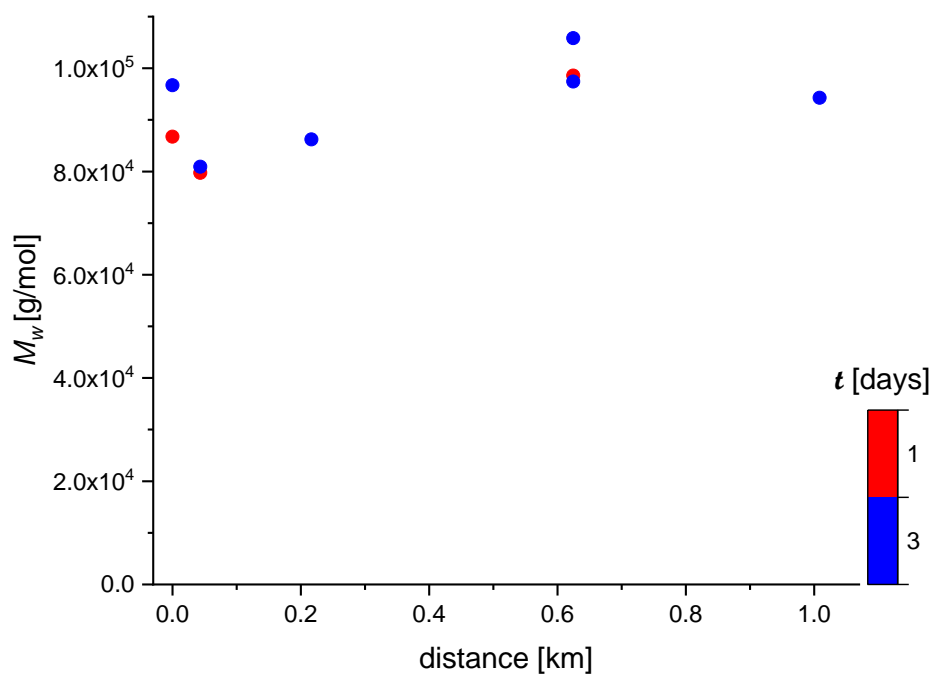


Figure 3.9: The weight average molecular weight of 2E5 did not change systematically over the course of the experiment.

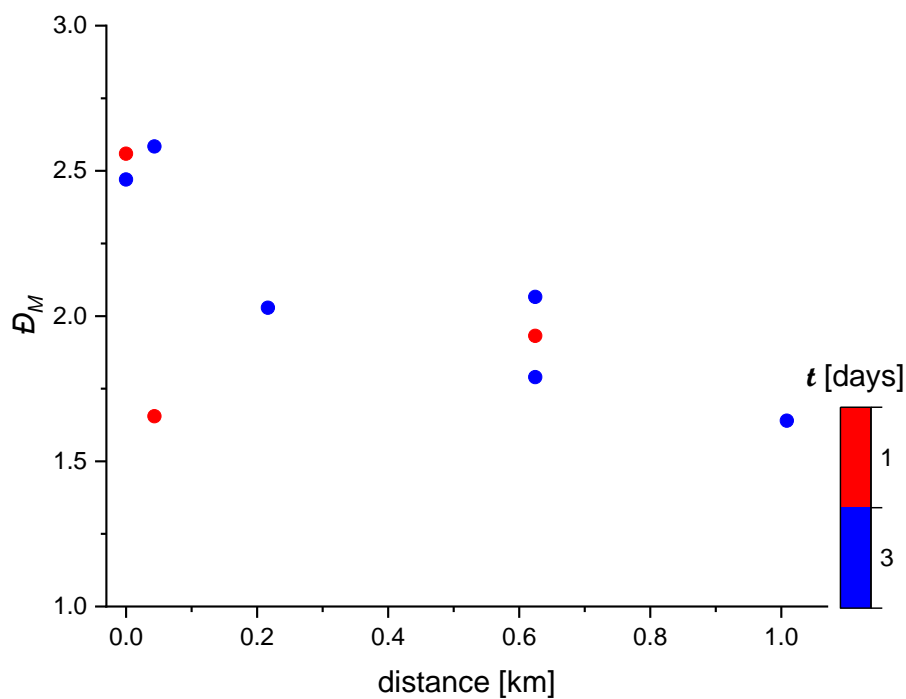


Figure 3.10: The molar mass dispersity indicated a broader molecular mass distribution for 2E5 compared to 4E6 (Fig. 3.8). For both polymers low values for  $M_n$  caused more random scatter in the  $D_M$ .

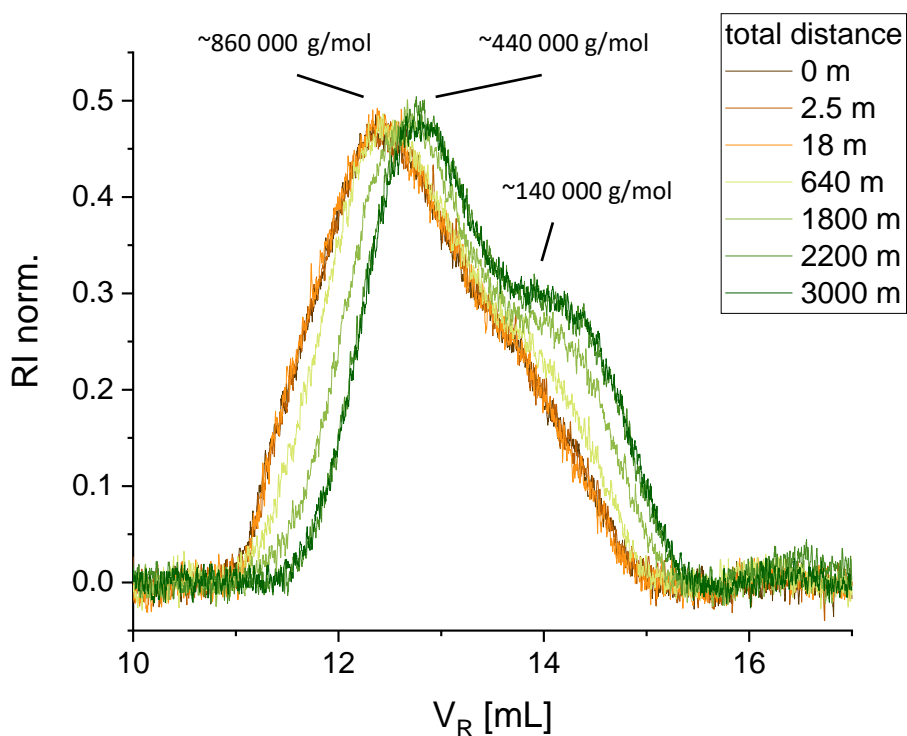


Figure 3.11: Chromatograms of 63 d old samples of 4E6. The samples differed in the distance they had travelled through the flow facility. The peaks were shifted to larger retention volumes (corresponding to a lower molecular weight) with increasing distance and a second peak was formed.

Chromatograms of 4E6 measured after 63 d are displayed in Fig. 3.11. At this time, the GPC-setup was improved: Two columns were used instead of one, providing better separation of different weight fractions. The normalized refractive index shows their relative weight distribution. Polymer samples that travelled less than 1 km through the flow facility and were stored for 63 days had their peak molecular weight at  $0.9 \cdot 10^6$  g/mol. With increasing distance travelled through the flow facility the shoulder observed at lower molecular weight became broader. For samples that travelled more than 2 km, the main peak was shifted to  $0.4 \cdot 10^6$  g/mol. The distribution indicates that the molecules were broken roughly in the middle of the chain, as reported in previous studies.<sup>[34]</sup> The distribution at 3 km was formed by chains that broke multiple times.

### 3.5 Untangling ageing and degradation

Examples of data sets used for the age-mapping are shown in Fig. 3.12. Each set contains the results of repeated GPC measurements of one sample. The sets differ in the distance the polymer has travelled through ViEDRA. Due to degradation in shear, samples that travelled longer distances had a lower  $M_w$ . The  $M_w$  of the polymers in one sample decreased with time. In order to untangle the contribution of shear and ageing degradation, an empirical mapping of samples of different age is performed. For most samples, the GPC measurements were performed some days after the sample was taken from ViEDRA. With the mapping, it is possible to account for the decay due to ageing, that happened between the taking of the sample and the GPC measurement (results in  $M_w$  at the day the sample was taken). In addition, it allows for the calculation of theoretical values for  $M_w$  and DR at the first day of the experiment (see appendix C).

The ageing was roughly exponential. The probability of dissociation should be the same for all bonds between the same elements in all molecules (different values for C-O and C-C bonds). This caused a constant relative decrease in molecular weight which results in a faster absolute decrease for larger molecules (the fragments of large molecule are much smaller compared to the original molecule, while

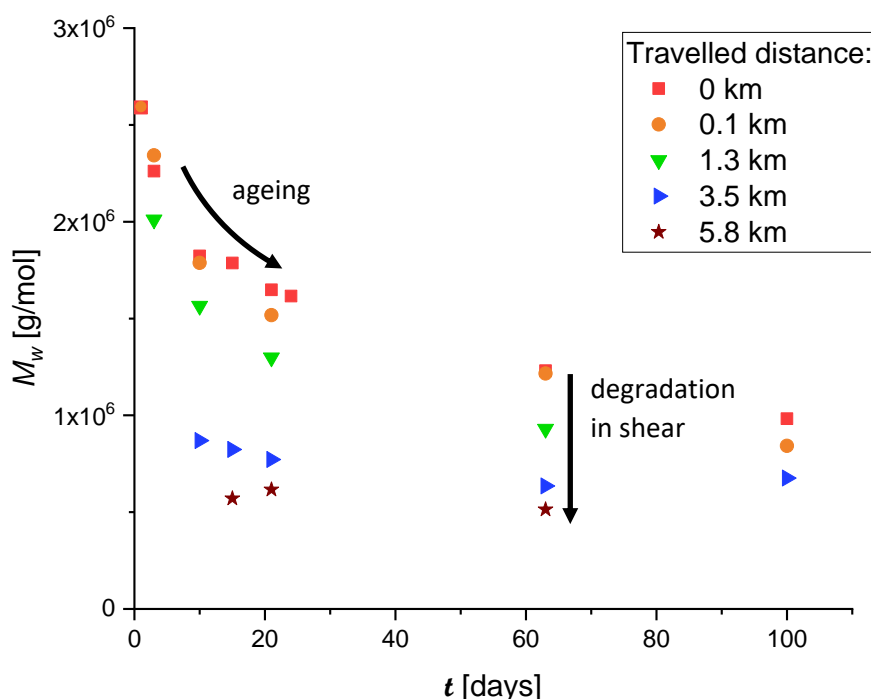


Figure 3.12: Decrease in the molar weight of the repeatedly measured samples. Samples which travelled longer distances through the flow facility started at lower  $M_w$ . At  $0.5 \cdot 10^6$  g/mol no further degradation due to age was detected.

the fragments of small molecules are in the same size range). It was assumed that the ageing only depends on  $M_w$  and is independent of the molecular weight distribution or the history of the sample. The molecular weight decreased towards a lower limit  $M_{w\infty}$ . Samples with  $M_w$  in the range of  $0.5 \cdot 10^6$  g/mol showed no or only minor degradation with time. An exponential decay function (Equation 3.1) was fitted to all samples which were measured multiple times, using empirical fit parameters  $A'$  and  $B$ . An adjusted age  $t_{adj.}$  was used, because the samples started at different molecular weights, depending on the distance they travelled through ViEDRA. This fit was only used to calculate  $M_{w\infty}$  (Equation 3.1). The mapping was improved by using relative values for the molecular weight and the age of a sample and using the square root of the age as independent coordinate (Equation 3.2).

$$M_w = B e^{-A' t_{adj.}} + M_{w\infty} \quad \text{Equation 3.1}$$

$$M_{w \text{ rel.}} = \frac{M_w - M_{w\infty}}{M_{w0} - M_{w\infty}} = e^{-A \sqrt{t_{\text{rel.}}}} \quad \text{Equation 3.2}$$

$$t_{\text{rel.}} = (\sqrt{t} - \sqrt{t_0})^2 \quad \text{Equation 3.3}$$

In Equation 3.2  $M_{w0}$  was the result of the first measurement of a sample, while  $M_{w\infty}$  was the lower limit of ageing, estimated by a fit of Equation 3.1.  $M_{w \text{ rel.}}$  was a measure how far the degradation of the polymer in a sample had proceeded compared to the first measurement of the sample. For each measurement it was calculated as the difference of  $M_w$  and  $M_{w\infty}$  relative to the molecular weight estimated in first measurement of the sample  $M_{w0}$ . The relative age of a sample  $t_{\text{rel.}}$  during a measurement was calculated using Equation 3.3, with  $t_0$  being the age of a sample at its first measurement and  $t$  the value at the current one. Because the half-life of a sample increased with decreasing molecular weight, the square root of the age of the sample was used as independent coordinate. This causes the slope of the decay to be directly proportional to  $M_w$ , allowing for the use of a relative age. Due to these definitions the first measurement of a sample could not be used for the fit ( $M_{w \text{ rel.}} = 1$ ,  $t_{\text{rel.}} = 0$ ). Only samples that were measured at least two times had an impact on the calculation. The decay parameter  $A$  determines how fast  $M_{w\infty}$  is reached.

The established fit is plotted in Fig. 3.13. In order for the graph to be linear, the y-axis is on logarithmic scale while the x-axis is the square root of the relative age. Some data points had to be excluded from the fit, because for samples that travelled long distances through the flow facility the difference between  $M_{w0}$  and  $M_{w\infty}$  was small, leading to an increased error in the calculation of  $M_{w \text{ rel.}}$  (grey points in Fig. 3.13). The parameters of the best fit are listed in Table 3.1.

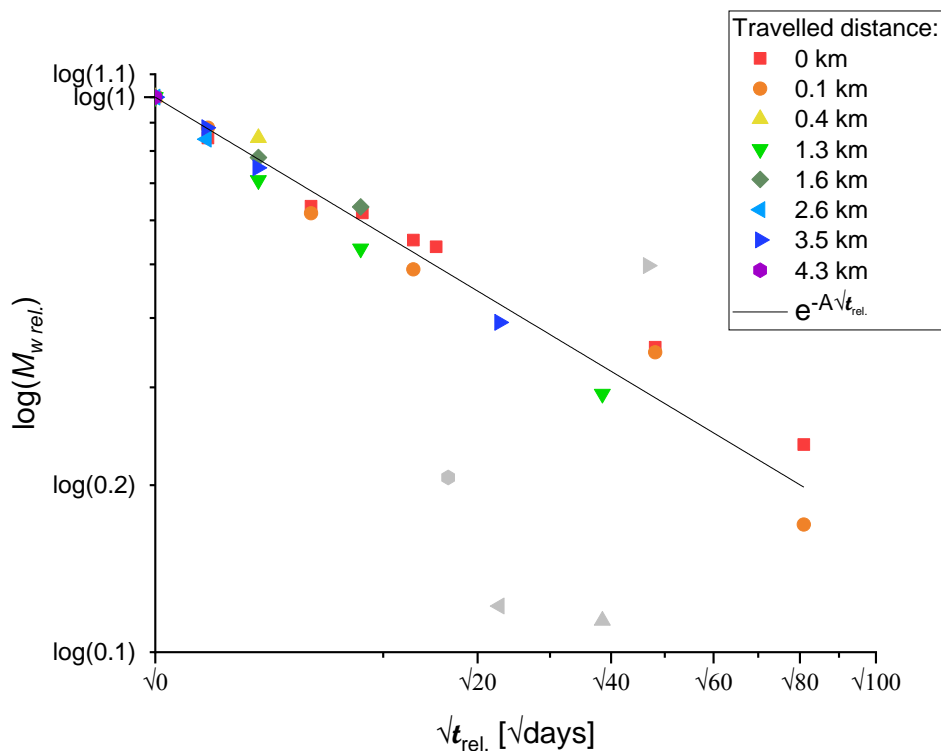


Figure 3.13: Fit of the relative molecular weight versus the relative age of a sample at each measurement. All samples were fitted using the same decay function, but some data-points had to be excluded due to an increased relative error.

Table 3.1: Parameters of the exponential ageing of the polymer, using  $M_w$  of the repeated GPC measurements.

Number of data points	$M_{w\infty}$ [g/mol]	A [1/vd]	$R^2$
22	$0.48 \cdot 10^6$	0.180	0.96

The age mapping was used to estimate the molecular weight of the polymer at the day the sample was taken from ViEDRA ( $M_{w0}$ ).  $M_{w0}$  was calculated, using the measured  $M_w$  and  $t_{rel.}$ . The relative age was calculated from the age of the sample at the day of the GPC experiment  $t$  and its age at the day it was taken  $t_0$ . For A and  $M_{w\infty}$  the values listed in Table 3.1 were used. The mapping caused the results of all measurements of one sample to collapse into one point, independent of their age (Fig. 3.14). Samples with a measured  $M_w$  smaller than  $M_{w\infty}$  could not be mapped. Due to the degradation in shear the molecular weight of those samples was already below the estimated lower limit of ageing  $M_{w\infty}$ . The model assumes that their molecular weight was not affected by ageing any more.

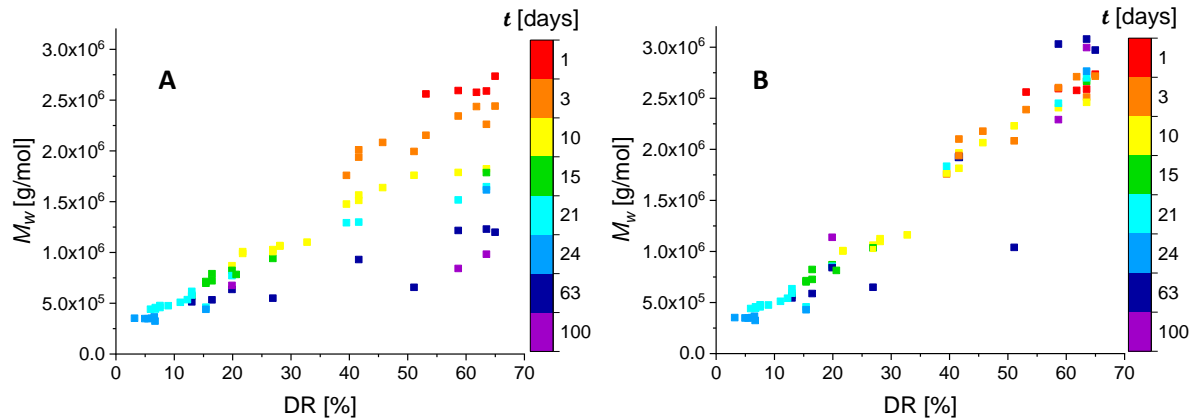


Figure 3.14: Relation of molecular weight and drag reduction without (A) and with (B) the age mapping. With the mapping, all measurements of one sample (corresponding to one x-position) gave roughly the same  $M_w$ .

The quality of the mapping can be seen in Fig. 3.14, in which the molecular weight of the polymer is plotted versus the drag reduction measured just before the sample was taken. If the molecular weight is not mapped (3.14 A),  $M_w$  decreased with age for each sample. Depending on the time elapsed between taking the sample and the GPC-measurement a different relation between  $M_w$  and drag reduction could be found. The second graph (3.14 B) shows the mapped results, as if the GPC measurements had been performed immediately after the samples had been taken from the flow facility. With the age mapping all measurements confirm the linear dependency of  $M_w$  and drag reduction.

### 3.6 Comparison of PEO with different molecular weight

The drag reduction efficiency of a polymer is related to its molecular weight. This dependency has been shown in multiple studies<sup>[2, 12, 35]</sup> and is the basis for models of polymer degradation in shear.<sup>[10, 23]</sup> In this work the weight average molecular weight was used to characterize the polymers. Compared to the number average molecular weight  $M_n$ ,  $M_w$  is less influenced by small molecular weight fractions. This causes the estimation of  $M_w$  to be less prone to instabilities, caused by random results in the light scattering of small molecules. However, previous studies have shown that the drag reduction efficiency depends not only on the average molecular weight, but on the weight distribution.<sup>[35]</sup> Small amounts of larger polymers can increase the drag reduction efficiency more than they increase  $M_w$ . Only the full weight distribution would provide information about all weight fractions relevant for drag reduction.

Fig. 3.15 shows  $M_w$  and the drag reduction efficiency. All samples of both 4E6 and 2E5 are included. As in Fig. 3.14,  $M_w$  is plotted versus the drag reduction measured in the last run before the sample was taken. For 4E6 the age correction was used to calculate the molecular weight at the date of the drag reduction measurement. Data points in light grey were GPC results of samples, which were 63 d old or older. The age correction was less reliable for samples of that age.  $M_w$  and DR showed a linear relationship over the course of the flow experiment. A linear fit of these results (GPC data of age 63 d and 100 d excluded) can be found in appendix C (Equation A.1). 2E5 deviated from this linear relation. It provided more drag reduction than the last samples of 4E6, despite having a smaller  $M_w$ . Different reasons could have caused this deviation:

- All samples of 2E5 had a high  $\mathcal{D}_M$ . Small amounts of larger molecules or polymer aggregates could have increased the drag reduction.
- The pipe-flow experiments of 2E5 and the degraded 4E6 resulted in a very small difference between the polymer solutions and pure water. Small errors in the estimated flow rate and pressure drop could have caused larger deviations for low values of drag reduction. If parameters changed between dates or different experiments (4E6, 2E5, water), all results in that group could be shifted systematically.

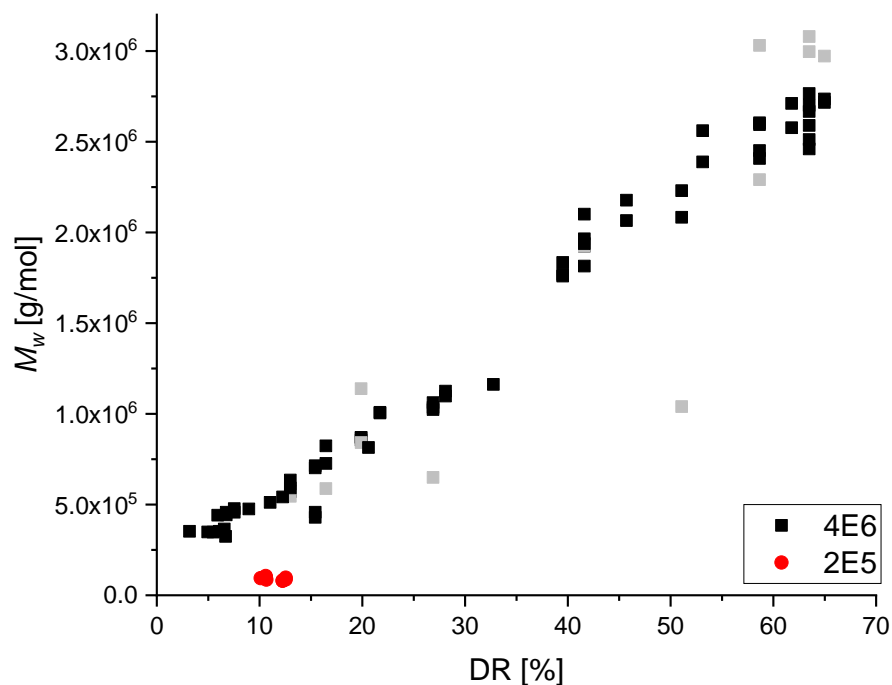


Figure 3.15: For 4E6 the drag reduction measured in the flow facility was directly proportional to  $M_w$ . 2E5 had a lower  $M_w$  than all samples of 4E6 but caused more drag reduction than the last of them.

### 3.7 Comparison of the measured polymer degradation with Brostow's model

The molecular weight of 4E6 and its drag reduction capability decreased during the experiment. In Brostow's model the drag reduction is directly proportional to the molecular weight of the polymer. Both quantities are taken relative to the results of the unsheared polymer, resulting in the same decay function (Equation 1.8). The function is plotted and compared with the results of the experiments (Fig. 3.16). For  $M_w$  the age mapping was used to estimate the molecular weight at the day of the drag reduction experiment. Due to the increased relative noise for low drag reduction and the absence of a confirmed lower limit, it was not possible to perform a fit of Equation 1.8 to the results of these experiments. Instead models with fixed values for  $W$  were fitted to the drag reduction results. These fits established with the results of the DR-measurements were then compared with the molecular weight of the polymer. The estimated parameters can be found in Table 3.2.

The number of weak points  $W$  determines the lower limit of drag reduction and the rate constant  $h_0$  governs how fast the lower limit is reached. With  $W = 16$  the decay stops at 6% of its starting value, corresponding to the drag reduction measured at the end of the flow facility experiment. Lower values of  $W$  can be ruled out, because the decay would have stopped at higher DR. However, a lower bound cannot be confirmed, because there were still changes in DR and  $M_w$  estimated in the last measurements. A second model with  $W = 60\,000$  was also compared to the results. Breaking PEO with a molecular weight of  $2.7 \cdot 10^6$  g/mol into  $C_2H_4O$  units (cleaving of C-O bonds) would result in about 60 000 fragments and would lead to a decrease towards virtual zero DR. Due to the adjustments of  $h_0$  the two models differ only slightly in their consistency with the experimental results.

In the logarithmic plot (Fig. 3.17), the absence of a lower limit in the measured drag reduction and  $M_w$  becomes visible. For DR the decrease at the end of the experiment was unclear because of the increased relative noise for low values of DR. Any decay after 10 km was smaller than the observed scatter. To confirm or rule out a lower bound of approximately 6%, experiments with a travelled distance up to 100 km would be needed (see Fig. 3.17).

Table 3.2: Parameters of the estimated decay functions.

	Number of data points	DR <sub>0</sub> [%]	$M_{w0}$ [g/mol]	$W$	$h_0$ [km <sup>-1</sup> ]	R <sup>2</sup>
<b>DR</b>	1282	65	-	16	$4.28 \cdot 10^{-2}$	0.95
				60 000	$1.04 \cdot 10^{-5}$	0.97
<b>M<sub>w</sub></b>	39	-	$2.7 \cdot 10^6$	16	$4.28 \cdot 10^{-2}$	0.92
				60 000	$1.04 \cdot 10^{-5}$	0.93

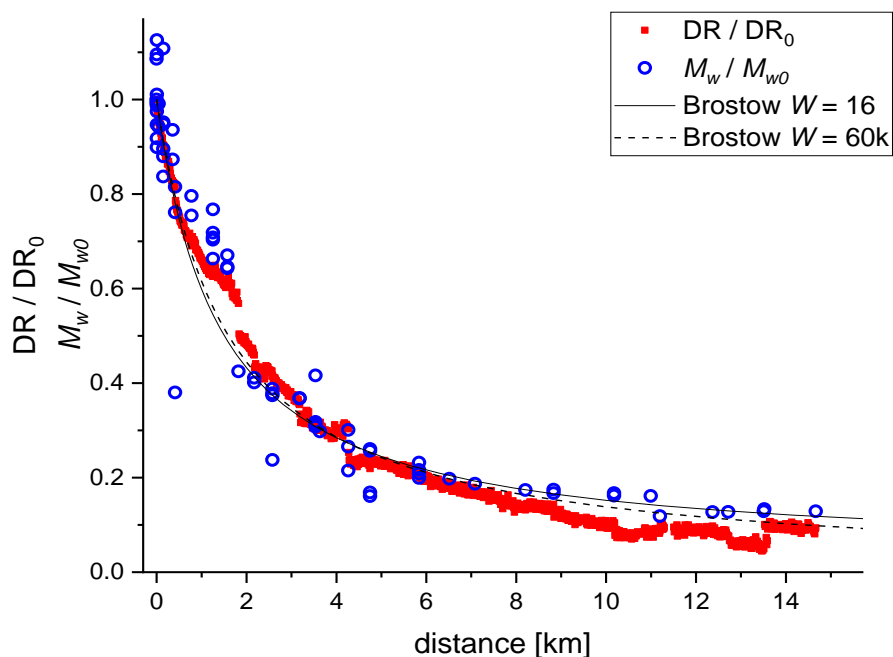


Figure 3.16: Comparison of the degradation of 4E6 with Brostow’s model. Drag reduction and  $M_w$  are plotted relative to the results of the first sample. Due to the adjustments of  $h_0$ , both models provide a reasonable fit of the results, independent of the number of weak points ( $W$ ).

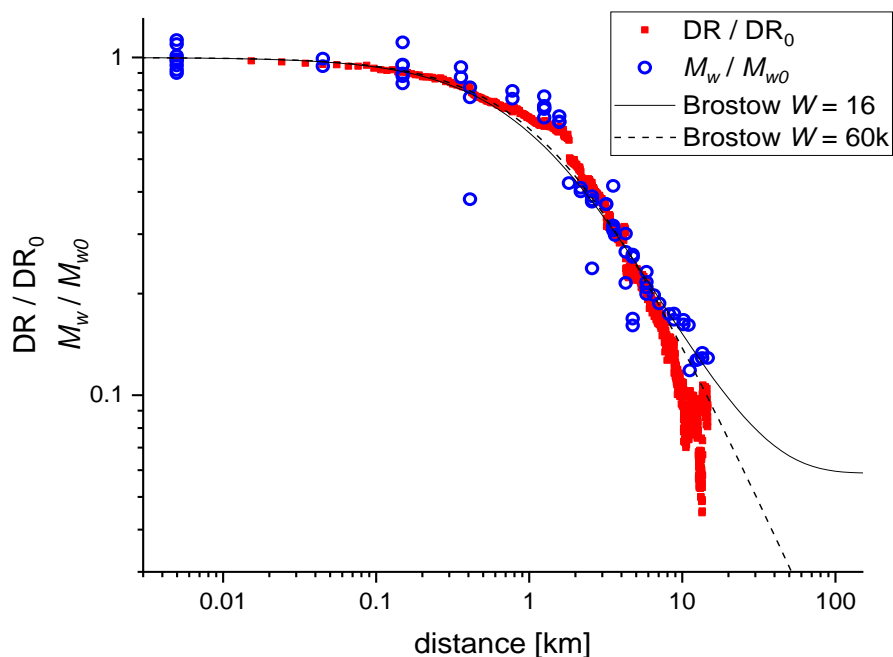


Figure 3.17: Logarithmic plot of polymer degradation. In a model with 16 breaking points the decay stops at 6% of its starting value. Increased random scatter at the end of the drag reduction measurements (red) make it hard to tell if the decay had come to a halt at 6% or would continue to lower values.

## 4. Summary and Outlook

The long term drag reducing properties of PEO were studied in a pipe-flow facility. Drag reduction up to 65% was found for 100 wppm PEO at  $Re = 10^5$ . DR decreased with the distance as the polymer travelled through pipes. After 2 km only half its starting value remained.

Measurements of the molecular mass of PEO revealed that in addition to polymer degradation in shear, ageing of the polymer solutions occurred. On a timescale of days, the molecular mass decreased towards a lower limit of  $0.5 \cdot 10^6$  g/mol, while the solutions were stored at ambient conditions. An exponential model was established in order to perform an age mapping and to estimate the molecular weight of PEO at different days. Change of the molecular weight dispersity differed for degradation in shear and ageing. This indicates a difference in the mechanism.

The measurements of drag reduction and molecular mass confirmed their linear relationship which is part of Brostow's model of the degradation of drag reducing agents. It was possible to approximate the results of the long-term experiment with this model. However, a lower bound of the degradation of PEO, as proposed in the model, could not yet be confirmed.

These results could be improved by testing the degradation in shear over even longer distances. Due to the small changes in the exponential decay, double the distance would be necessary to see systematic changes. In addition, a better control of  $Re$  in ViEDRA would help to improve the estimation of DR. For low values of DR, scans over a small  $Re$ -range could be performed in order to provide results that are comparable between all runs.

During the experiment, the control software of ViEDRA was improved. In future experiments it will be possible to perform more runs in less time. This reduces the influence of ageing of the polymer solutions. Equal long term drag reduction experiments should also be conducted with different polymers.

## Bibliography

- [1] Toms, B. A. (1948). Some Observations on the flow of linear polymer solutions through straight tubes at large Reynolds numbers. 1st International Congress in Rheology.
- [2] Virk, P. S. (1975). "Drag reduction fundamentals." *AIChE Journal* 21(4), 625-656.
- [3] Burger, E. D., et al. (1982) "Flow Increase in the Trans Alaska Pipeline Through Use of a Polymeric Drag-Reducing Additive." *Journal of Petroleum Technology* 34(2).
- [4] Hoyt, J. W., Taylor, J. J., Altman, R. L. (1980). "Drag Reduction—Jet Breakup Correlation with Kerosene-Based Additives." *Journal of Rheology* 24, 685.
- [5] Singh RP, Singh J, Deshmukh SR, Kumar D. (1995). "Application of drag-reducing polymers in agriculture." *Current science*; 68(6), 631-631.
- [6] Sellin, R. H. J., Ollis, M. (1980). "Polymer Drag Reduction in Large Pipes and Sewers: Results of Recent Field Trials." *Journal of Rheology* 24, 667.
- [7] Fabula, A. G. (1971). "Fire-Fighting Benefits of Polymeric Friction Reduction." *Journal of Basic Engineering* 93(3), 453-455.
- [8] Funkhouser, G. P., Norman, L. R., (2002). Methods of fracturing subterranean zones penetrated by well bores and fracturing fluids therefor. US Patent No. 6,986,391.
- [9] Hong, C. H., Jang, C. H., and Choi, H. J. (2015). "Turbulent Drag Reduction with Polymers in Rotating Disk Flow." *Polymers* 7, 1279-1298.
- [10] Zhang, X., Duan, X., Muzychka, Y. (2018). "New mechanism and correlation for degradation of drag-reducing agents in turbulent flow with measured data from a double-gap rheometer." *Colloid and Polymer Science*, 296, 829–834.
- [11] Keller, A., Kiss, G., and Mackley, M. (1975). "Polymer Drag Reduction in Taylor Vortices." *Nature*, 257(5524), 304–305.
- [12] Vanapalli, S. A., Islam, M. T., Solomon, M. J. (2005). "Scission-induced bounds on maximum polymer drag reduction in turbulent flow." *Physics of Fluids* 17 095108.
- [13] Escudier, M., Presti, F., and Smith, S. (1999). "Drag Reduction in the Turbulent Pipe Flow of Polymers." *Journal of Non-Newtonian Fluid Mechanics* 81(3), 197–213.
- [14] Zadrazil I. (2011). Various Aspects of Polymer Induced Drag Reduction in Turbulent Flow. Imperial College London.
- [15] Gasljevic, K., Aguilar, G., and Matthys, E. (1999) "An Improved Diameter Scaling Correlation for Turbulent Flow of Drag-Reducing Polymer Solutions." *Journal of Non-Newtonian Fluid Mechanics*, 84(2-3), 131–148.
- [16] Moussa, T. and Tiu, C. (1994) "Factors Affecting Polymer Degradation in Turbulent Pipe-Flow." *Chemical Engineering Science*, 49(10), 1681–1692.

- [17] Smith, R. and Tiederman, W. (1991) "The Mechanism of Polymer Thread Drag Reduction." Rheologica Acta, 30(2), 103–113.
- [18] den Toonder, J., Draad, A., Kuiken, G., and Nieuwstadt, F. (1995) "Degradation Effects of Dilute Polymer-Solutions on Turbulent Drag Reduction in Pipe Flows." Applied Scientific Research, 55(1), 63–82.
- [19] White, C. M. and M. G. Mungal (2008). "Mechanics and Prediction of Turbulent Drag Reduction with Polymer Additives." Annual Review of Fluid Mechanics 40(1), 235-256.
- [20] Xi, L. (2019) "Turbulent drag reduction by polymer additives: Fundamentals and recent advances." Physics of Fluids 31(12), 121302.
- [21] Le Brun, N., et al. (2016). "On the drag reduction effect and shear stability of improved acrylamide copolymers for enhanced hydraulic fracturing." Chemical Engineering Science 146, 135-143.
- [22] Hunston, D. L., and Zakin, J. L. (1980). "Flow-assisted degradation in dilute polystyrene solutions" Polymer Engineering and Science 20(7), 517-523.
- [23] Brostow, W. (1983). "Drag reduction and mechanical degradation in polymer solutions in flow." Polymer 24(5), 631-638.
- [24] Reynolds, O. (1883). "An experimental investigation of the circumstances which determine whether the motion of water shall be direct or sinuous, and of the law of resistance in parallel channels," Philosophical Transactions of the Royal Society of London, 174, 935-982.
- [25] Virk, P., Merrill, E., Mickley, H., and Smith, K. (1967). "The Toms Phenomenon: Turbulent Pipe Flow of Dilute Polymer Solutions." Journal of Fluid Mechanics, 30(2), 305–328.
- [26] Berman, N. (1978). "Drag Reduction by Polymers." Annual Review Fluid Mechanics, 10, 47-64
- [27] Brennen, C., Gadd, G. E. (1967). "Aging and Degradation in Dilute Polymer Solutions," Nature, 215, 1368–1370.
- [28] Nakken, T., Tande M., Nyström B. (2004). „Effects of molar mass, concentration and thermodynamic conditions on polymer-induced flow drag reduction." European Polymer Journal, 40, 181-186.
- [29] Bossard, F., et al. (2010). "Influence of dispersion procedure on rheological properties of aqueous solutions of high molecular weight PEO." Rheologica Acta 49:529-540.
- [30] Cox, R., Dunlop, E. (1977) "Influence of Molecular Aggregates on Drag Reduction." Physics of Fluids, 20(10), 203–213.
- [31] Müller, H. W., et al. to be published
- [32] International Association for the Properties of Water and Steam, (2008) "Release on the IAPWS Formulation 2008 for the Viscosity of Ordinary Water Substance." available at <http://www.iapws.org>.

[33] Kotliar, A. M. (1963). "Evaluation of Molecular Weight Averages Resulting from Random Crosslinking and Chain Scission Processes for Wide Schulz-Zimm Distributions." Journal of Polymer Science: Part A, 1, 3175-3182.

[34] Buchholz, B. A., et al. (2004). "Flow-induced chain scission as a physical route to narrowly distributed, high molar mass polymers." Polymer 45, 1223-1234.

[35] Figueiredo, M. S., et al. (2007). "Development of a Method to Evaluate the Performance of Aqueous Polymer Solutions as Drag Reduction Agents in Bench Scale." Macromolecular Symposia, 245–246, 260–265.

[36] Berman, N. (1997). "Drag reduction of the highest molecular weight fractions of polyethylene oxide." The Physics of Fluids 20(5) 715-718.

## Appendix A: GPC calibration

In order to calibrate the GPC-system PEO standards were used. They were purchased from Agilent. Each of the two vials contained PEO of four different molecular weights. Table A.1 lists the properties of the polymers. The second peak of the green standard ( $M_w = 32080$  g/mol) was used to perform the calibration. The calibrated method was then verified by analysing the other peaks.

In Fig. A.1  $M_w$  (GPC) is plotted versus the retention volume of each peak. It was possible to use the calibrated method to calculate  $M_w$  of three peaks of the yellow standard and of two peaks of the green standard. For the smaller polymers, the signals obtained in the light-scattering detectors were too low to use them in the calculation.  $M_w$  calculated with the method accords with the values stated by Agilent and the plot of  $\log(M_w)$  versus retention volume results in a straight line for all of them.

Table A.1: GPC-calibration standards provided by Agilent.

Vial Code	IV [dL/g]	$M_w$ [g/mol] (light scattering)	$M_n$ [g/mol] (GPC)	$M_w$ [g/mol] (GPC)	$M_w/M_n$ (GPC)	$M_p$ [g/mol] (GPC)	Mass/vial [mg]
yellow	5.3938	875 000	668 500	774 000	1.16	863 500	0.2
	0.9752	80 400	68 850	71 650	1.04	73 550	0.4
	0.1310	3 580	3 730	3 830	1.03	3 870	0.6
	-	-	-	-	1.00	194	0.8
green	4.4063	622 000	493 500	550 500	1.12	552 000	0.2
	<u>0.4963</u>	<u>31 050</u>	<u>30 390</u>	<u>32 080</u>	<u>1.06</u>	<u>32 790</u>	<u>0.4</u>
	0.0680	1 490	1 410	1 470	1.04	1 480	0.6
	-	-	-	-	1.00	106	0.8

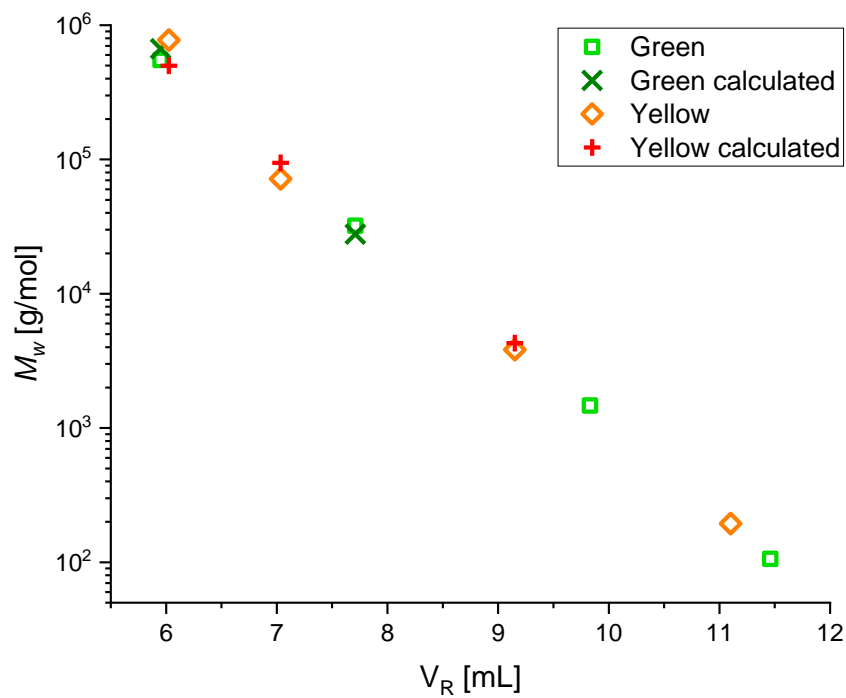


Figure A.1: GPC results of the calibration standards. The molecular weights calculated using the calibration and the values stated by Agilent show the expected linear relationship of  $\log(M_w)$  and the retention volume of the peak.

## Appendix B: Detailed results in Couette-Taylor flow

In Fig. A.2 and Fig. A.3 the flow behaviour of water and some polymer solutions in circular double gap geometry is shown. Between shear rates of  $160 \text{ s}^{-1}$  and  $190 \text{ s}^{-1}$  all samples transitioned from Couette-flow to Taylor-flow. This caused a rapid increase in nominal shear viscosity due to the formation of Taylor vortices. The shear onset of Taylor-flow and overall viscosity was increased by the presence of PEO, depending on the molar weight of the polymer. 2E5 gave a viscosity profile similar to pure water. For 4E6 the shape depended on the distance, the polymer chains had run through the flow facility (Fig. A.3). The first sample (0 km) had much higher viscosity than the later samples and the polymer also caused shear thinning in the Couette regime. The viscosities used in section 3.3 were calculated as the mean value of the Rheometer-results obtained before the onset point of Taylor-flow.

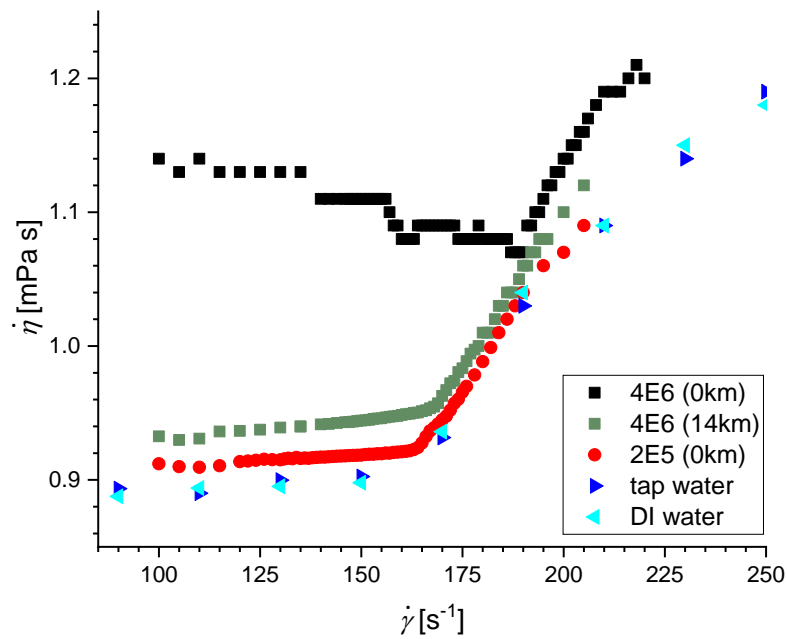


Figure A.2: Nominal shear viscosity of different samples in the tested shear rate range at. All liquids transitioned from Couette-flow to Taylor-flow. The presence of polymer caused an increase in viscosity and shifted the onset point of Taylor-flow to higher shear rates. For 4E6 the effect depended on the distance the polymer chains in the sample had travelled through ViEDRA.

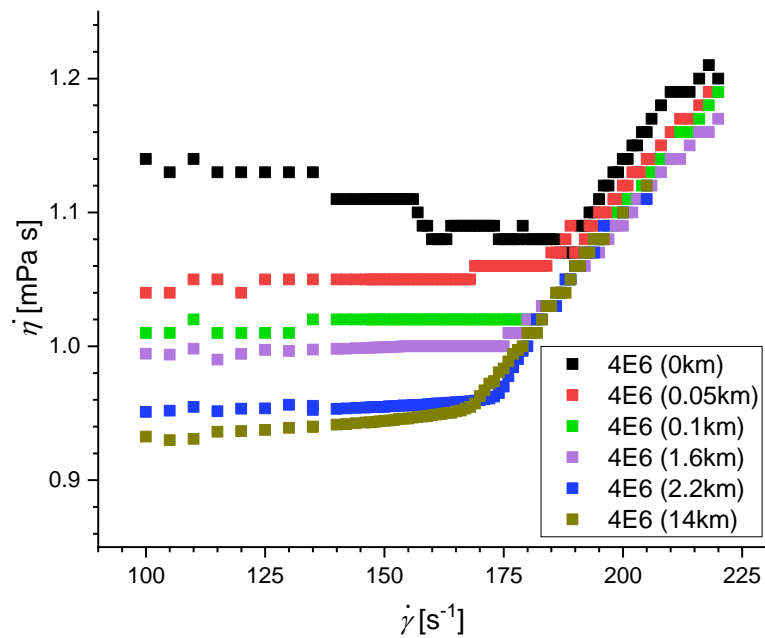


Figure A.3: Viscosity of 4E6 samples taken at different points of the drag reduction experiment. The viscosity of the polymer solutions decreased with increasing distance travelled through ViEDRA. This indicated degradation of the polymer.

## Appendix C: Age mapping

The age mapping obtained with the results of the repeated GPC-measurements was used to calculate theoretical results for drag reduction and  $M_w$  that would have been measured, if all experiments were performed during one day. Similar to how the mapping was applied in section 3.5, the exponential function was used to calculate  $M_{w0}$ , using the measured  $M_w$  and the age of the sample at the day of the experiment  $t$ . The parameter  $t_0$  was 1 for all samples in order for  $M_{w0}$  to be the molecular weight at the first day.

However, this calculation method contains a small systematic error: The degradation during drag reduction experiments depends on the molecular mass, causing faster degradation for bigger molecules. If all experiments would have been performed during one day, almost no decrease in  $M_w$  due to ageing would have happened. This would have led to a higher  $M_w$  during the runs that were performed during the later days in the real experiment. The higher  $M_w$  would have caused faster degradation, leading to an  $M_w$  slightly lower than calculated with the age mapping.

In order to apply the mapping to the results of the drag reduction experiments the linear relation of drag reduction and  $M_w$  was utilised. A linear function was fitted to the results of 4E6 shown in Fig. 3.15 ( $M_w$  versus DR, GPC measurements of age 63 days and 100 days excluded), resulting in an empirical dependency shown in Equation A.1 ( $R^2 = 0.981$ ). This equation was used to convert the measured drag reduction into  $M_w$ , which was then adjusted with the age mapping before converted back. The calculation is shown in Equation A.2, where  $t$  is the age of the solution at the day of the drag reduction experiment,  $DR_t$  is the result of that experiment and A is the decay parameter introduced in section 3.5. The mapping was not applied for DR-values that resulted in an  $M_w$  below  $M_{w\infty}$ .

$$\frac{M_w}{\text{g/mol}} = 4.13 \cdot 10^6 \cdot \text{DR} + 7.94 \cdot 10^4 \quad \text{Equation A.1}$$

$$\text{DR}_{\text{day 1}} = \frac{(4.13 \cdot 10^6 \cdot \text{DR}_t + 7.94 \cdot 10^4) - M_{w\infty} - 7.94 \cdot 10^4 + M_{w\infty}}{4.13 \cdot 10^6} e^{-A \cdot (\sqrt{t}-1)} \quad \text{Equation A.2}$$

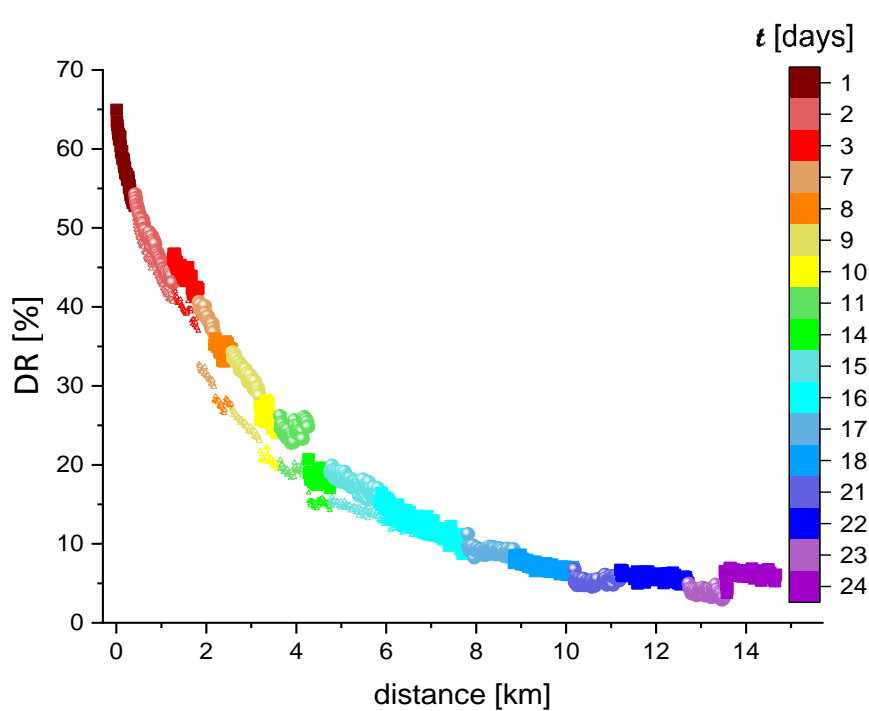


Figure A.4: Comparison of the drag reduction with (big points) and without (small points) the age mapping. The results between day 2 and day 17 are shifted to higher values by the mapping.

The effect of this age mapping is shown in Fig. A.4. The small points are the drag reduction results as obtained from the flow facility; the big points are corrected with the age mapping. At first the difference between the two increases, as the age-mapping gets more important with increasing age of the solution. It reaches its maximum at day 9. When the molecular weight calculated from the drag reduction comes closer to  $M_{w^\infty}$ , the difference decreases again. For measurements after day 17 the mapping was not applied, because the calculated  $M_w$  was below  $M_{w^\infty}$ .

With the age mapping the step between the results of day 3 and day 7 disappears. However, the step between day 11 and day 14 does not change and an additional step after day 2 is introduced. The additional step is due to the increased  $Re$  of the runs on day 3 which is visible in Fig. 3.4. The step from day 11 to day 14 is also accompanied by a change in  $Re$ .

The age mapping has minor influence on the parameters in the fit of Brostow's model. The increased values of DR for distances between 1 km and 6 km causes a small decrease of the parameter  $h_0$ . The parameter  $W$  is not affected, because the drag reduction at the end of the experiment is not changed by the age correction. Fits of the model with the calculated results of DR and  $M_w$  at day 1 are shown in Fig. A.5 and Fig. A.6, the parameters listed in Table A.1.

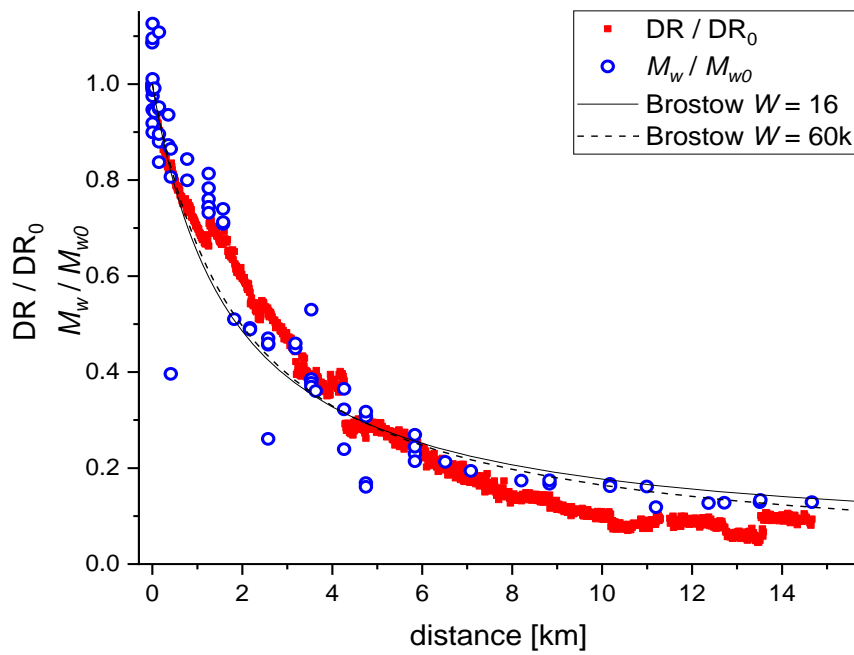


Figure A.5: Brostow’s model compared to drag reduction and  $M_w$  adjusted by the age mapping. Only the parameter  $h_0$  is affected.

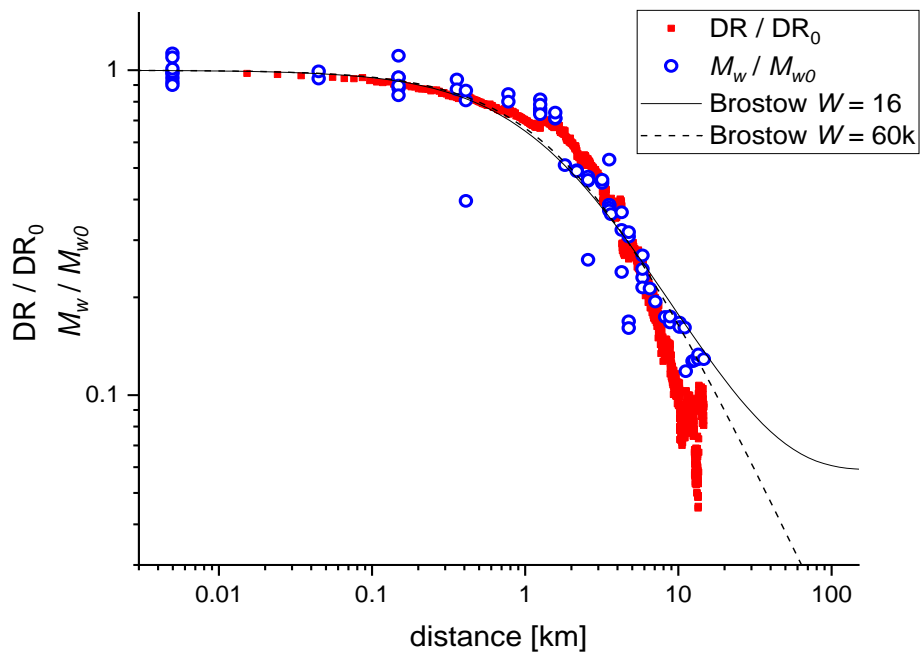


Figure A.6: Logarithmic plot of the comparison. Only minor change is caused by the age mapping because DR and  $M_w$  at the beginning and at the end of the experiment are not affected.

Table A.1: Parameters of the estimated decay functions for the results adjusted by the age-mapping.

	Number of data points	DR <sub>0</sub> [%]	$M_{wo}$ [g/mol]	$W$	$h_o$ [km <sup>-1</sup> ]	R <sup>2</sup>
<b>DR</b>	1282	65	-	16	$3.43 \cdot 10^{-2}$	0.92
				60 000	$8.47 \cdot 10^{-6}$	0.94
<b>M<sub>w</sub></b>	39	-	$2.7 \cdot 10^6$	16	$3.43 \cdot 10^{-2}$	0.91
				60 000	$8.47 \cdot 10^{-6}$	0.92

## English Abstract

To reduce the drag in turbulent flow of liquids, drag reducing agents can be added to the system. These can be polymers with long, flexible chains that are soluble in the liquid. Drag reducing agents are already used in industrial applications in order to save energy while pumping and to reach higher flow-velocities. A challenge in their application is the degradation of polymers in turbulent flow which results in a decreased drag reduction. In this study the properties of polyethylene oxide were monitored, while it was used as a drag reducing agent. In a pilot scale pipe-flow facility aqueous solutions of the polymer were pumped repeatedly, simulating the application in a kilometre long pipeline. The drag reduction was measured and samples of the solution were taken at multiple times. The molecular weight of the polymer of these samples was measured. A decrease in drag reduction with distance travelled through the flow facility was found. This concurs with results found in previous studies and also mostly with the model suggested by Brostow. The model proposes a lower bound for drag reduction in long term applications. This bound could not be confirmed for polyethylene oxide, but the results show, that it has to be at a very low value. In addition, ageing of the polymer solutions was found, while they were stored at ambient conditions. The molecular weight of polyethylene oxide decreased with time, despite it was not subjected to mechanical stress.

## Deutsche Zusammenfassung

Um den Strömungswiderstand in turbulenten Strömungen von Flüssigkeiten zu verringern, können der Flüssigkeit Drag Reducing Agents zugesetzt werden. Dies können Polymere mit langen, flexiblen Ketten, die in der jeweiligen Flüssigkeit löslich sind, sein. Um Energie beim Pumpen zu sparen und höhere Fließgeschwindigkeiten zu erreichen werden sie bereits vielfach in der Industrie eingesetzt. Problematisch ist aber der Umstand, dass die Polymere durch die Scherkräfte im turbulenten Fluss während der Anwendung abgebaut werden und dadurch die Drag Reduction mit der Zeit abnimmt. In dieser Arbeit wurden die Eigenschaften von Polyethylenoxid untersucht, während es als Drag Reducing Agent eingesetzt wurde. In einer Testanlage wurden wässrige Lösungen des Polymers mehrfach durch ein Rohr gepumpt, um die Anwendung in einer kilometerlangen Pipeline zu simulieren. Dabei wurde die Drag Reduction gemessen und wiederholt Proben gezogen, in denen die molare Masse des Polymers bestimmt wurde. Gefunden wurde eine Abnahme der Drag Reduction und der molaren Masse mit zunehmender Distanz, die die Lösung in der Testanlage zurückgelegt hat. Dies stimmt mit Ergebnissen in der Literatur und größtenteils auch mit Brostows Modell überein. Brostows Modell sagt eine untere Grenze für die Drag Reduction in Langzeitanwendungen voraus, die in diesem Experiment für Polyethylenoxid nicht bestätigt werden konnte, aber bei sehr niedrigen Werten liegen müsste. Zusätzlich wurde eine Alterung der Polymerlösungen gefunden, während diese in Ruhe gelagert wurden. Die molare Masse von Polyethylenoxid nahm mit der Zeit ab, ohne dass das Polymer mechanischem Stress ausgesetzt war.